



# Compressive and tensile behaviour of concrete subjected to high rate of loading

Mohammad Mohsin Khan<sup>1</sup> · Kamran<sup>1</sup> · Mohd Ashraf Iqbal<sup>1</sup>

Received: 17 August 2023 / Accepted: 8 December 2023 / Published online: 2 January 2024  
© Springer Nature Switzerland AG 2024

## Abstract

The present study describes the dynamic tensile and compressive behaviour of concrete with respect to failure (damage) and material characteristics. The dynamic compression and tension tests were performed by using the Split Hopkinson Pressure Bar setup of 65 mm diameter of bars. The cylindrical specimen tested under dynamic loading conditions was ~ 30 mm in length with two different diameters (30 mm and 45 mm). The quasi-static compressive and splitting tensile strength of concrete was found to be 49.48 and 5.42 MPa, respectively. Dynamic testing showed a significant 78% increase in compressive strength as the strain rate increased from  $1.33 \times 10^{-4}$  to  $284 \text{ s}^{-1}$ . Likewise, tensile strength increased by approximately 303.4% when the strain rate increased from  $6.67 \times 10^{-4}$  to  $14.95 \text{ s}^{-1}$ , demonstrating concrete high strain rate sensitivity to dynamic tension. Under dynamic compression, the concrete strength increases due to the formation of the large number of cracks and high lateral confinement. In addition, the crushing density of concrete specimens has been increased with an increase in strain rate. During dynamic tensile failure, the specimen split into two semi-cylindrical pieces at low strain rate. Concurrently, localized crushing occurred at a high strain rate due to stress concentration at loading points. As the strain rate increased further, it intensified the localized crushing, ultimately giving rise to the formation of a wedge region followed by crushing zone.

**Keywords** Split Hopkinson Pressure Bar (SHPB) · Strain rate effect · Dynamic increase factor · High-speed photography · Failure mechanism · Fragmentation

## Introduction

Impact studies have traditionally focused on military applications, impact load generated by incoming missile on bunkers and ammunition storage structures, and important structures. Dynamic loading from the natural hazards like tornadoes, earthquakes, ocean waves, etc., is also an important form of high load and high strain rate point of view. Vehicle impact, missile impact, projectile or aircraft impact, and impact on important concrete structures, i.e. nuclear power plants, hospitals, schools, and bunkers, are the prime examples of high

loading rate conditions generating a demand to study the dynamic behaviour of concrete structures. The impact of ships and vehicles on reinforced concrete (RC) structures is a critical consideration in structural engineering. In marine environments, ships generate dynamic loads during berthing and mooring operations, subjecting the adjacent RC structures to substantial forces. The effects include localized stress concentrations and potential structural damage. Similarly, vehicular loads from traffic on bridges and parking structures can lead to fatigue and degradation of the concrete over time. Engineers must meticulously design RC structures to withstand these dynamic forces, incorporating factors such as material strength, impact resistance, and appropriate reinforcement to ensure the longevity and safety of the infrastructure in the face of maritime and vehicular impacts [1–4]. The damage identification techniques demand increasing significantly to identified the damage localization and quantification of the structural elements [5]. Identification of the weak location of RC column subjected to barge impact is so critical in analysis and design

✉ Mohammad Mohsin Khan  
mkhan@ce.iitr.ac.in

Kamran  
kamran@ce.iitr.ac.in

Mohd Ashraf Iqbal  
ashraf.iqbal@ce.iitr.ac.in

<sup>1</sup> Department of Civil Engineering, Indian Institute of Technology, Roorkee 247667, India

of structures. The investigation revealed that the areas near the base, impact point, and upper section of the RC column exhibit the most significant damage due to a barge collision, primarily attributed to the presence of significant bending moments in these specific regions [6]. Therefore, the novel frame-type crashworthy devices have been implemented on the RC piers for the protection under vehicle collisions [7]. Engineering materials like metals, concrete, composite, and ceramics are frequently subjected to high rate of deformation during the service life. The researchers are constantly and systematically working to advance the properties of materials to acquire the necessary physical characteristics which are suitable for high rate of loading conditions. Based on the literature studies [8–10], it has been concluded that the properties of concrete under high strain rates are highly intricate, exhibiting significantly distinct dynamic response patterns and damage mechanisms when compared with its behaviour under quasi-static loading conditions. In the last decade, the utilization of concrete has become popular for safety and security purposes such as it essentially contributes towards structural integrity and human protection. Thus, to gather comprehensive information, the study of dynamic complex behaviour of concrete and its failure mechanism with respect to the crushing and cracking that occurred due to impact or blast load becomes essential for the investigation and design of strategic structures of concrete.

Various experimental methods, such as hydraulic testing machines, drop weight impact test, SHPB test, flyer impact test method, and plate impact test, are employed to explore the impact of high strain rates on the mechanical properties of concrete. Among them, the SHPB technique stands as the dominant and commonly employed approach for investigating the dynamic properties of brittle and ductile materials, enabling the exploration of strain rates ranging from 100 to 10,000  $s^{-1}$  under conditions of uniaxial compression [11]. The ASTM [12] and ISRM [13] suggested the Brazilian disc test calculate the splitting tensile strength of concrete and rock materials subjecting uniaxial quasi-static tension, respectively. Further, the researchers extended the splitting tensile test approach in the Split Hopkinson Pressure Bar test to evaluate the dynamic splitting tensile response of concrete [14–17]. Therefore, the Split Hopkinson Pressure Bar (SHPB) method has found extensive application in the dynamic assessment of concrete properties subjected to both compression and splitting tensile loading conditions.

The dynamic increase factor (DIF) is used to quantify the strain rate dependency of material properties and is defined as the ratio of dynamic compressive strength to quasi-static compressive strength of material. Bischoff and Perry [8], Pajak [10], and Malvar and Ross [18] performed the comprehensive study by using the experimental data available in the literature on concrete and other cement-based materials subjected to high strain rates, to evaluate the high strain

rate effect and concluded that the compressive and tensile strength of concrete significantly increased with an increase in the strain rate. However, no discussions were conducted regarding the failure pattern, fragmentation, and failure mechanisms of the materials under dynamic conditions. Furthermore, the dynamic tensile strength is more sensitive to the strain rates than the dynamic compressive strength hand observing a significant increase in tensile strength nearly thirteen times the quasi-static tensile strength [10, 18], while there was a lack of explanation regarding the failure mechanism and failure pattern of material. Rissgaard et al. [19] described that the behaviour of concrete has the transition strain rate, which distinguishes the variation in concrete strength beyond the transition strain rate, observed drastic increment in the dynamic strength, and the DIF in compression varied from 1 to about 3.5. Brara and Klepaczko [20] performed experiments on the dry and wet microconcrete by using SHPB and concluded that the DIF for dry microconcrete varies from 4 to 13, while, for the wet microconcrete, the DIF varies from 4 to 8 when the loading rate varies from 800 to 5000 GPa/s, but the failure mechanism along with initiation and propagation of crack were not explained experimentally.

Li and Mang [21] conducted an experimental and numerical investigation using the Split Hopkinson Pressure Bar (SHPB) on materials exhibiting characteristics like brittle concrete. Their numerical findings indicated that the dynamic strength of these concrete-like materials is enhanced due to the pseudo-strain rate effect or structural effect, a structural influence that is responsive to the hydrostatic stress induced by lateral inertia confinement. The presence of the pseudo-strain rate effect could result in an overestimation of the dynamic numerical strength in comparison with the actual strength of the material. Nard and Bailley [22] described that the increase in dynamic compressive strength of concrete was mainly attributed to the lateral inertia confinement (structural effect) rather than the effect of strain rate. In other words, the DIF is primarily caused by the inertial force generated due to the structural effect rather than the strain rate effect (material effect). Also, Cotsovos and Pavlovic [23] described that the DIF obtained from the dynamic loading conditions is mainly caused by the inertial force owned by lateral inertia confinement describing the structural effect. On the other hand, the experimental study performed on the cylindrical concrete specimen through the SHPB test by Tang et al. [24] concluded that the strain rate had a significant influence on both the dynamic compressive strength and critical strain at failure, whereas the lateral inertia confinement effect was too small and insignificant, and it could be ignored. The previous studies have described comprehensively about the potential factors leading to contributing in concrete strength enhancement under a high rate of loading. However, a detailed experimental

explanation regarding the failure mechanism of concrete must be explored yet for describing its damage behaviour under dynamic loading.

The dynamic failure modes are entirely different from the quasi-static with respect to the crack propagation phenomena such that the transgranular propagation of cracks phenomena occurred in concrete describing the cracking of aggregate under high strain rate, while the intergranular propagation of cracks occurred in the concrete at quasi-static strain rate and crack propagated through the Interface Transition Zone (ITZ) [25–28]. The mechanism behind the axial crushing phenomena, which occurred in concrete specimens during dynamic compression test, is defined as the concrete getting crushed and broken into fragments. Initially, the size of fragments would be bigger at low strain rate loading, and the size of fragments keeps decreasing with an increase in the strain rate resulting in a higher number of fragments [25–27]. Under the dynamic splitting tensile test, the concrete specimen mainly fails into two semi-cylindrical pieces across the diameter of the specimen and is crushed at the contact points due to the high loading rate [29–31]. However, there is a need for in-depth investigation to ascertain the mechanism behind the crack initiation and propagation, and the occurrence of local crushing. Further research is required to explore the influence of varying strain rates under tension on the concrete damage and failure modes.

Apart from its impact on material properties and structural integrity, fire can also have significant consequences for structures and their components, especially when subjected to blasts or explosions. In the event of a blast, a fireball, intense heat, high temperatures, and a shockwave can collectively impose extensive damage on building infrastructure and its materials. The amalgamation of blast effects and subsequent fire is commonly termed a fire dynamic load. The effects of fire on the materials of a structure and its elements can be quite severe. The elevated temperatures generated by the fire can weaken or even melt structural materials like steel or concrete, resulting in structural failure due to a significant decrease in compressive, tensile, and shear strength [32, 33]. The heat-induced expansion and subsequent contraction create a loading and unloading scenario, leading to warping, buckling, or the collapse of building components [34, 35]. Therefore, it is imperative to incorporate the effects of high temperature into the DIF for materials, necessitating an in-depth study.

Dynamic material characterization of concrete is of dominant significance in understanding its behaviour under varying loading conditions, such as blast, impact, or seismic forces. Unlike static tests, dynamic tests provide insights into the dynamic response of materials to rapid and dynamic loading, offering a more accurate illustration of real-world situations. This research aids in designing structures with enhanced durability and safety, particularly in defence

applications, impact, and blast conditions. By analysing dynamic properties like stiffness, damping, and strain rate sensitivity, researchers can develop advanced models for predicting concrete performance under dynamic forces, contributing to the optimization of construction materials and techniques for improved infrastructure durability.

The concrete structures experienced significant damage due to the occasionally occurring accidental (dynamic) loading conditions such as seismic, impact, blast, and explosive loads describing the need for the study pertaining to the dynamic behaviour of concrete material. Previous research has not sufficiently addressed the damage caused to concrete by high loading rates, particularly in terms of the cracking and crushing of the concrete material. Therefore, a thorough and profound investigation has been required to found a strong understanding about the damage of concrete, failure pattern, and the failure mechanism to describe the enhancement of the concrete strength under the high rate of loading.

The primary objective of this study is to gain a deeper insight into how high strain rates influence the dynamic material characteristics of concrete. The dynamic properties were defined in terms of the dynamic compressive and tensile strengths, DIF, stress–strain curves, energy absorption properties, failure mechanism, and fragmentation. These investigations are conducted through experimental tests utilizing the Split Hopkinson Pressure Bar (SHPB) setup. High-speed photography was employed to monitor the failure mechanism, generation of cracks, and propagation of cracks. Additionally, a comprehensive analysis of the tested specimens has been conducted to investigate the mode of failure. This analysis includes examining the weight of the crushed specimen, its shape, and the number of fragments produced. Moreover, we have correlated the concrete crushing data with the strain rate to examine the impact of high-rate loading on fragmentation.

## Materials and methods

A design for the concrete mix was conducted to establish the ingredient proportions in compliance with the standards IS 10262:2019 [36] and IS 456: 2000 [37]. The mixture incorporated Ordinary Portland Cement (OPC) of 43 grade with a specific gravity of 3.15. Coarse aggregates (CA) have a maximum size of 9–10 mm and 2.63 specific gravity. Naturally dried sand is used as the fine aggregate (FA) sieve with the standard sieve of 4.75 mm, having 2.42 specific gravity. BASF Master Glenium 51 is used as a superplasticizer with 1.08 specific gravity. The ratio of concrete ingredients for M45 grade of concrete was 1:1.97:1.97 (Cement: FA: CA) and 0.40 water/cement ratio calculated using the weigh-batching method. The concrete cubes of size 150 mm were prepared for quasi-static compression testing, and the

cylindrical shape specimens with different aspect ratios were extracted from these cubes for dynamic material characterization. The core cutting machine is employed to extract concrete cores from these cubes. Three different core cutters were used in the present study for extracting the cores that had diameters of 30 and 45 mm. The concrete cores were subsequently cut to height ( $L \approx 30$  mm) to maintain the aspect ratio ( $L/D$ ) of 0.7 and 1. The minimum dimension of the cylindrical specimen should not be less than the three times the maximum size of coarse aggregates (CA); hence, the specimen height should be at least 28 mm [36].

### Quasi-static compression and splitting tensile test

Quasi-static compressive and tensile experiments were conducted to determine the quasi-static concrete strength for comparison of the DIF of strength. The 150-mm size cubes were cast and cured for 28 days at 25–30 °C temperature and tested on a universal testing machine (UTM) as per IS 516:1959 [38]. The quasi-static compression test was conducted on the concrete cubes and carried out under displacement-controlled conditions at a rate of 0.02 mm/s, which is equivalent to a strain rate of  $1.3 \times 10^{-4} \text{ s}^{-1}$ . The average compressive strength of three cubes was obtained as 49.48 MPa with a 2.67 MPa standard deviation and 0.54 coefficient of variance. The modulus of elasticity obtained using the IS 456: 2000 [33] is 33.54 GPa ( $E_c = 5000\sqrt{f_{ck}}$ ).

Three different methods were accepted to investigate the quasi-static tensile strength of concrete, i.e. direct tensile test, modulus of rupture test (three-point bending method), and splitting tensile test (Brazilian disc). The Brazilian disc test is the most acceptable method to determine the tensile strength for quasi-static strain rates ranging from  $10^{-7}$  to  $10^0 \text{ s}^{-1}$  [13]. This method is the simple, easy to perform, and gives more accurate splitting tensile strength results. In this method, the cylindrical specimen was inserted between two Brazilian discs with a longitudinal axis perpendicular to the loading direction and placed between the plates of the testing machine, see Fig. 1a. Based on the elasticity theory,

the two-dimensional stress acting on the element near the centre along the vertical specimen diameter is determined by using the following equations, see Fig. 1b;

$$\sigma_x = \frac{2P}{\pi LD} \quad (1)$$

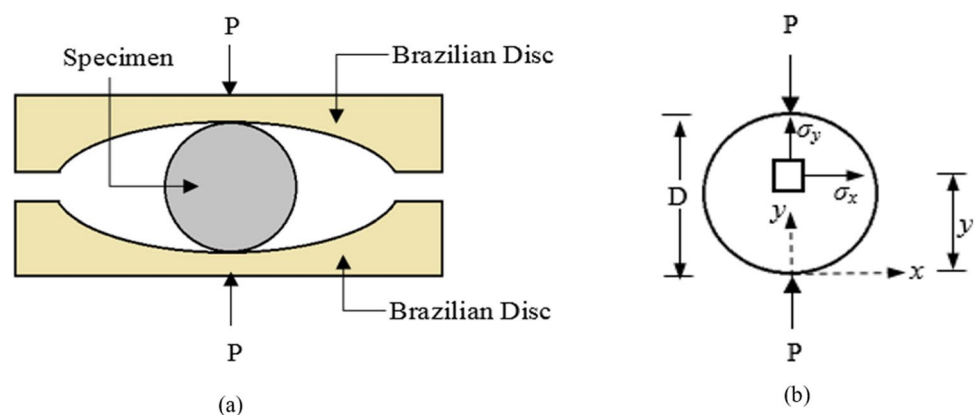
$$\sigma_y = \frac{2P}{\pi LD} \left[ \frac{y^2}{y(D-y)} - 1 \right] \quad (2)$$

where  $\sigma_x$  is horizontal tensile stress,  $\sigma_y$  vertical compressive stress,  $P$  compressive load at failure,  $L$  cylindrical specimen length,  $D$  specimen diameter, and  $y$  is the element distance from the loading ends. Equations (1) and (2) were only used to calculate the maximum tensile and compressive strength. The failure strain and stress–strain curve cannot be obtained by splitting tensile test [41]. In the present study, cylindrical concrete specimens with an aspect ratio ( $L/D$ )  $\approx 1$  were used, and tests were performed at a 0.02 mm/sec displacement rate. The average splitting tensile strength was 5.42 MPa with a 0.33 MPa standard deviation, and 0.060 coefficient of variance after 28 days of casting and curing, while the tensile strength calculated using IS 516: 1959 [38] is 4.69 MPa.

### Dynamic test

The SHPB method is employed to study the dynamic properties of brittle materials such as concrete, composites, and ceramics at high strain rates. The basic design idea of the SHPB setup to investigate the dynamic material properties was proposed by Kolsky [39] and the improvement suggested by Chen and Song [11] to increase the accuracy and preciseness of the experimental results. The schematic diagram of the SHPB setup used for dynamic characterization is illustrated in Fig. 2a. The experimental setup used to perform the dynamic tests is shown in Fig. 2b. The concrete specimens were placed along the length for the dynamic compression test and along the diameter for the dynamic splitting tensile test as shown in Fig. 2c and d, respectively.

**Fig. 1** Brazilian disc test **a** schematic view and **b** free body diagram of specimen



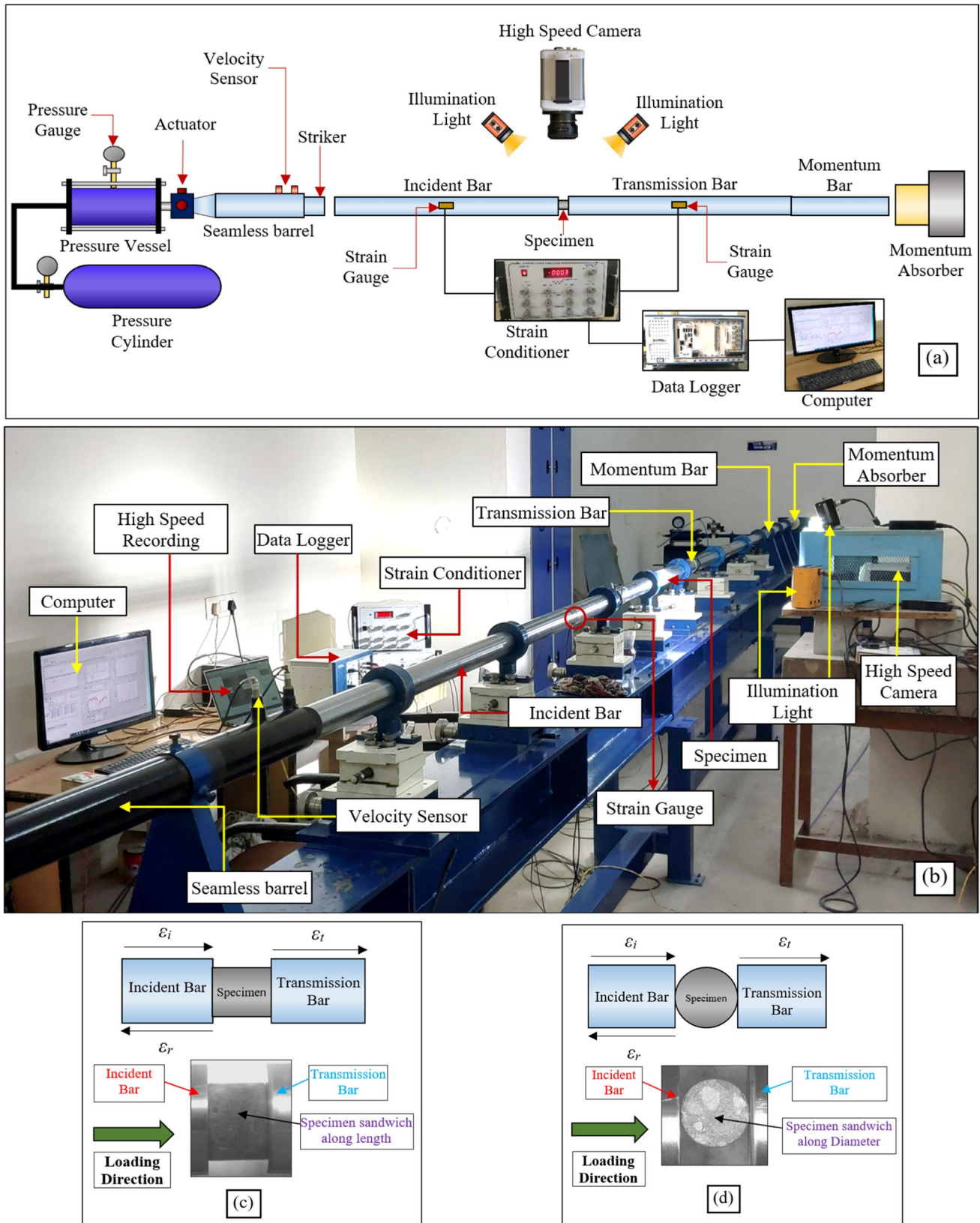


**Fig. 2** a Schematic diagram of SHPB, b experimental setup for dynamic test, c experimental arrangement for dynamic compression test, and d experimental arrangement for dynamic tensile test

A detailed description of the developed SHPB has been given in our previously published manuscript [40].

The seamless and smooth barrel of the gas gun propelled the striker bar, accelerating the striker bar towards the incident bar. This action caused an impact of striker on the incident bar, generating a trapezoidal shape compressive stress pulse wave within the incident bar. Upon reaching the stress pulse at the interface between the incident bar and the specimen, a portion of the incident wave reflects in the incident bar due to the distinct mechanical impedance of concrete and steel. The portion of the compressive stress wave that reflects is denoted as a reflected wave, whereas the remaining portion of the incident wave propagates through the specimen and enters the transmission bar, known as the transmitted wave. The incident wave strain  $\epsilon_I$  and reflected wave strain  $\epsilon_R$  were recorded at the centre of the incident bar, while the transmitted wave strain  $\epsilon_T$  recorded at the centre of the transmission bar by using the 3-mm length strain gauges paste at the centre of bars with the help of Data Acquisition and Recording System (DAQS), respectively. The bars must remain linear elastic and centric during the dynamic test. The working principle for dynamic compression and dynamic splitting tensile test is the same, only the difference in the placement of the cylindrical specimen. The specimen was placed along the length/thickness for the dynamic compression test (see Fig. 2c), while for the splitting tensile test, specimens were placed along the diameter (see Fig. 2d).

By utilizing the 1-D elastic stress wave propagation theory within the bar, Hook's law, and maintaining stress equilibrium in the specimen throughout the testing process, the stress, strain, and strain rate-time profiles in the specimen under compression loading were derived through the application of the subsequent equation;

$$\sigma_{cd} = E_b \left( \frac{2A_b}{A_s} \right) (\epsilon_I + \epsilon_R + \epsilon_T) = E_b \left( \frac{A_b}{A_s} \right) \epsilon_T \tag{3}$$

$$\epsilon_c = \frac{C_o}{L_o} \int_0^t (\epsilon_I - \epsilon_R - \epsilon_T) dt = -\frac{2C_o}{L_o} \int_0^t \epsilon_R dt \tag{4}$$

$$\dot{\epsilon}_c = \frac{C_o}{L_o} (\epsilon_I - \epsilon_R - \epsilon_T) = -\frac{2C_o}{L_o} \epsilon_R \tag{5}$$

where  $\sigma_{cd}$ ,  $\epsilon_c$ , and  $\dot{\epsilon}_c$  are the dynamic compressive stress (MPa), strain, and strain rate (1/s) in the specimen, respectively.  $A_b$  and  $A_s$  are the bars and specimen cross-sectional areas in  $\text{mm}^2$ , respectively.  $E_b$  is Young's modulus of elasticity of the pressure bar, and  $C_o$  is the pressure wave velocity in the pressure bar.  $L_o$  is the length of the specimen.

The splitting tensile test was also performed on cylindrical concrete along the diameter by using the SHPB apparatus. If the dynamic stress equilibrium condition is achieved

during test, the dynamic splitting tensile strength of concrete is directly proportional to the maximum value of the wave strain in the transmission bar, and strength is calculated by using the following equation;

$$\sigma_{td} = \left( \frac{E_b D_b^2}{2L_o d_s} \right) (\epsilon_I + \epsilon_R) = \left( \frac{E_b D_b^2}{2L_o d_s} \right) \epsilon_T \tag{6}$$

where  $\sigma_{td}$  is the dynamic splitting tensile strength (MPa) and  $D_b$  and  $d_s$  are the diameter of bars and concrete specimen in  $\text{mm}^2$ , respectively. The strain rate varies within the specimen during loading, so we use the average strain rate and loading rate in dynamic splitting tensile testing by using the following equations [14];

$$\dot{\epsilon}_t = -\frac{\sigma_t}{E_s T} \tag{7}$$

$$\dot{\sigma}_t = -\frac{\sigma_t}{T} \tag{8}$$

where  $\dot{\epsilon}_t$  is the tensile strain rate (1/s),  $E_s$  is the Young's modulus of elasticity of specimen,  $\dot{\sigma}_t$  is the loading rate in the specimen (GPa), and  $T$  is the time interval between the start and maximum occurrence of the transmitted wave. The experimental results demonstrated that the elastic modulus of concrete is not strain rate sensitive; therefore, the quasi-static elastic modulus is used in Eq. (7) to determine the strain rate [41]. In this research, the high strain rate tests were performed on the SHPB setup developed in the Civil Engineering Department, IIT Roorkee [40]. The incident and transmission bars have the similar geometrical configuration, and each bar has a 2990 mm in length and 65 mm in diameter, having an aspect ratio of 46:1, while the absorption and striker bars have 1500 mm and 200 mm lengths, respectively. All the bars were made of steel 4340 grade with  $190 \times 10^3$  MPa modulus of elasticity ( $E_b$ ), a density ( $\rho$ ) of 7850  $\text{kg/m}^3$ , and a Poisson's ratio of 0.3.

## Results and discussion

### Recorded signals and dynamic equilibrium condition

The striker impact velocity varies from 3 to 12 m/s, controlled by varying the compressed gas in the vessel to vary the strain rate in the concrete specimen. The sandwich specimen was prepared skillfully and carefully to maintain the perfect contact between bars and specimen end faces. A lubricant was applied at the interfaces of the specimen and bar to minimize the end friction. A specially designed LabVIEW program was used to perform the dynamic tests with

the required experimental conditions. The incident reflected and transmitted strain waves were recorded at a 1 million sample rate, and a 40-kHz cut-off frequency low-pass filter was used to remove the noise from the recorded signals. The filtered signals obtained from DAQS in strain–time format for dynamic compression and dynamic tension are shown in Figs. 3a and b, respectively.

The wave signal, once filtered, is segmented individually to extract specific portions corresponding to the incident, reflected, and transmitted signals. These segmented signals are then employed to analyse the equilibrium state condition, stress–time, strain–time, strain rate–time, and, ultimately, the dynamic stress–strain relationship of the specimen subjected to high strain rate loading. In order for the Split Hopkinson Pressure Bar (SHPB) test to be valid, it is essential that stresses should be evenly distributed along the length of the

specimen, and the specimen should attain equilibrium conditions throughout the dynamic testing process. Achieving the equilibrium condition in an SHPB test is essential to obtain reliable and accurate data on the dynamic behaviour of materials, especially at high strain rates. The ideal overlapping of  $I + R$  (incident wave + reflected wave) and  $T$  (transmitted wave) waves cannot be achieved during the SHPB test. Hence, the best overlapping curves achieved for equilibrium conditions obtained will be considered. The dynamic equilibrium condition in specimen is usually examined by the submission of incident strain pulse and reflected strain pulse should approximately coincide with the transmitted strain pulse, i.e.  $\epsilon_I + \epsilon_R = \epsilon_T$ . The equilibrium condition obtained in the present study for dynamic compression and tension test is illustrated in Fig. 4a and b, respectively. The peak strain values recorded are approximately 163.1 microstrains

**Fig. 3** Incident and transmission bar signals **a** dynamic compression test, **b** dynamic tensile test

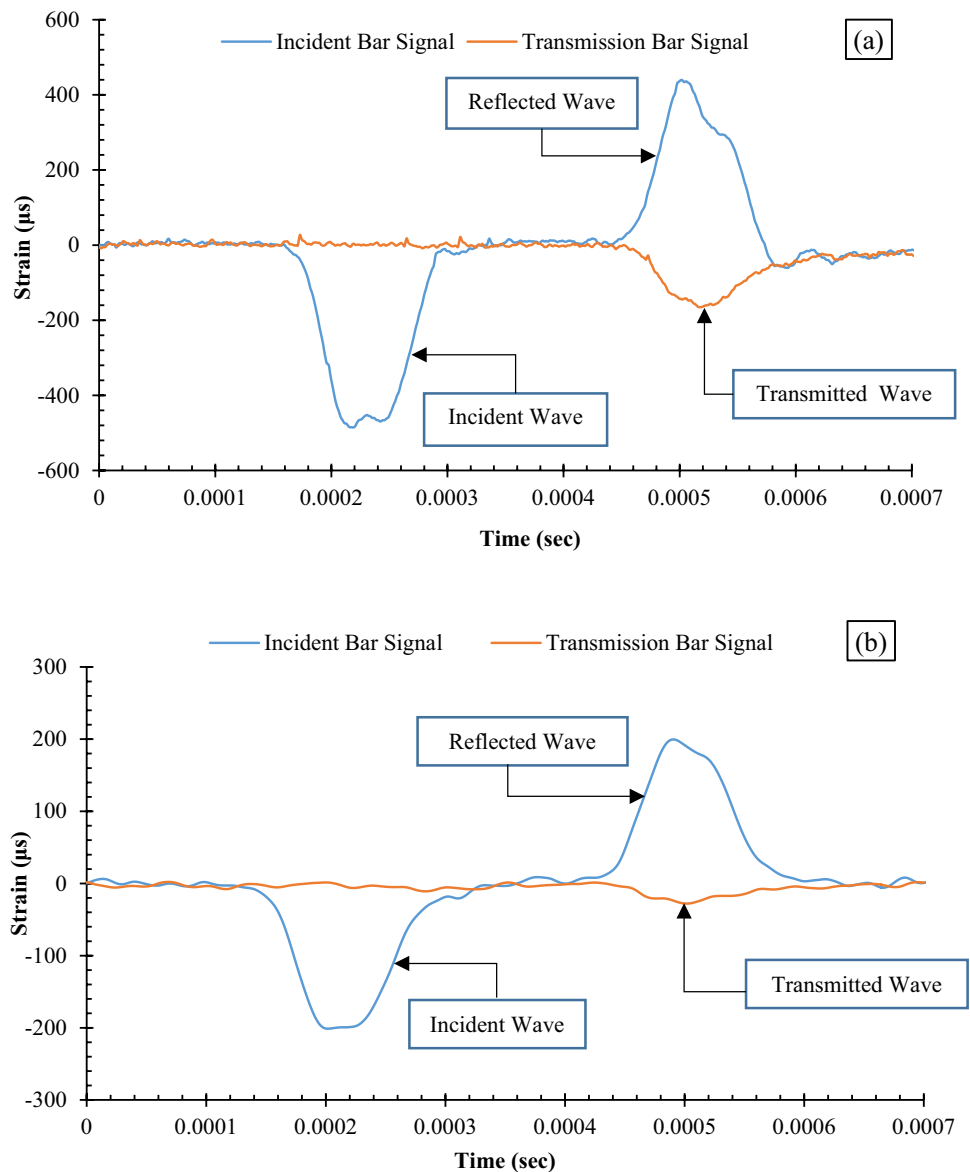
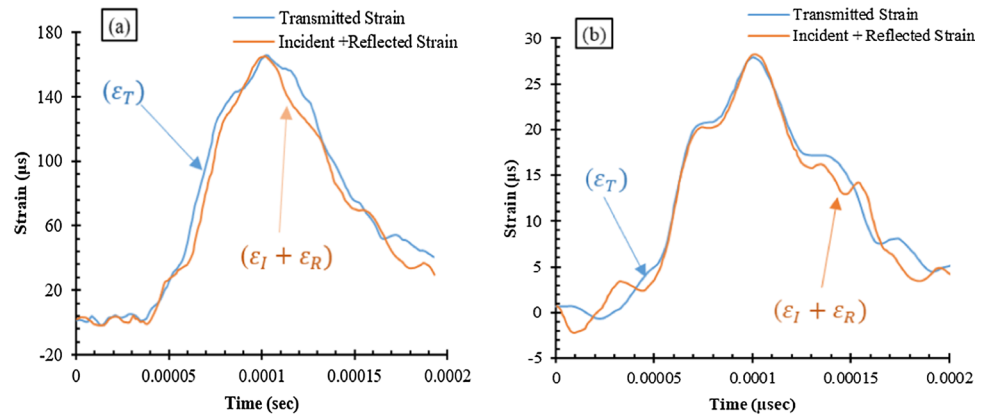


**Fig. 4** Dynamic equilibrium condition **a** compression test, **b** tensile test



for dynamic compression and 28.2 microstrains for tension equilibrium conditions. However, the strain amplitude in tension is significantly lower than in compression due to the lower splitting tensile strength of concrete as compared to its compressive strength, resulting in the transmission of a smaller portion of the incident wave. The experimental data and results are only valid until the stress equilibrium is achieved in the specimen.

### Dynamic compressive behaviour of concrete

#### Strain rate effect on dynamic compressive strength and DIF

Brittle materials are highly sensitive to the strain rate, but the strain rate does not remain constant during the failure process. To define the actual strain rate, the peak strength is used as the ultimate strength, while the strain rate at the corresponding instant of time is used as the representative strain rate at failure [26]. The thickness of the cylindrical specimens is ~30 mm in length; hence, the striker impact velocity was varied to change the strain rate in the specimen. Table 1 lists the dynamic compressive properties of the tested specimen fulfilled the equilibrium condition. The maximum and minimum dynamic compressive strength was

observed as 57.52 MPa and 88 MPa, corresponding to 72 and 284 s<sup>-1</sup> strain rates, respectively. The increasing trend of compressive strength with the increased strain rate was observed; see Fig. 5a. Under high-rate loading, the generated cracks propagate through the robust coarse particles (aggregate) and increase the concrete strength due to the higher stiffness of aggregates in the concrete matrix. The quantity of formation of microcracks also increased with an increase in strain rate, which further increases the strength under a high strain rate. As the strain rate increases, the generated crack response time is further reduced, and the intensity of localized failure further increases the dynamic strength [42]. In addition, the lateral inertia confinement also restrains the lateral deformation of the specimen due to inertia force generated in opposite direction of lateral deformation, which further increases the compressive strength. As well as, the inertia confinement increased with an increase in strain rate and affects the dynamic material properties significantly [44].

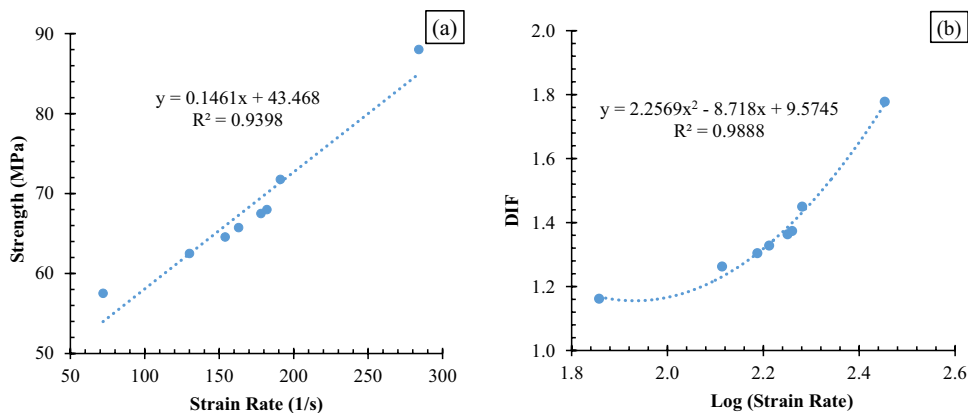
Most researchers [21, 25, 28, 40, 43] used the DIF to quantify the strain rate sensitivity of materials. In the present study, the DIF values obtained for the concrete in compression are listed in Table 1. An increasing trend of DIF with respect to log strain rate was observed and following the

**Table 1** Dynamic compressive properties at high strain rates

Sample ID	Strain rate	Peak stress	Peak strain	DIF	Pre-peak energy density	Post-peak energy density	Total energy density
	(1/s)	(MPa)		$(\frac{f_{cd}}{f_{cs}})$	(J/m <sup>3</sup> )	(J/m <sup>3</sup> )	(J/m <sup>3</sup> )
S1-L30-D30	72	57.52	0.002407	1.16	0.114	0.175	0.289
S2-L30-D45	130	62.50	0.00219	1.26	0.161	0.200	0.360
S3-L30-D45	154	64.60	0.002218	1.30	0.121	0.396	0.517
S4-L30-D30	163	65.74	0.002638	1.33	0.146	0.390	0.536
S5-L30-D45	178	67.5	0.002324	1.36	0.138	0.410	0.548
S6-L30-D45	182	68	0.002744	1.38	0.159	0.446	0.605
S7-L30-D30	191	71.77	0.002613	1.45	0.162	0.488	0.650
S8-L30-D30	284	88	0.002312	1.78	0.172	0.758	0.930



**Fig. 5** Dynamic compressive behaviour of concrete **a** compressive strength–strain rate, **b** DIF–log (strain rate)



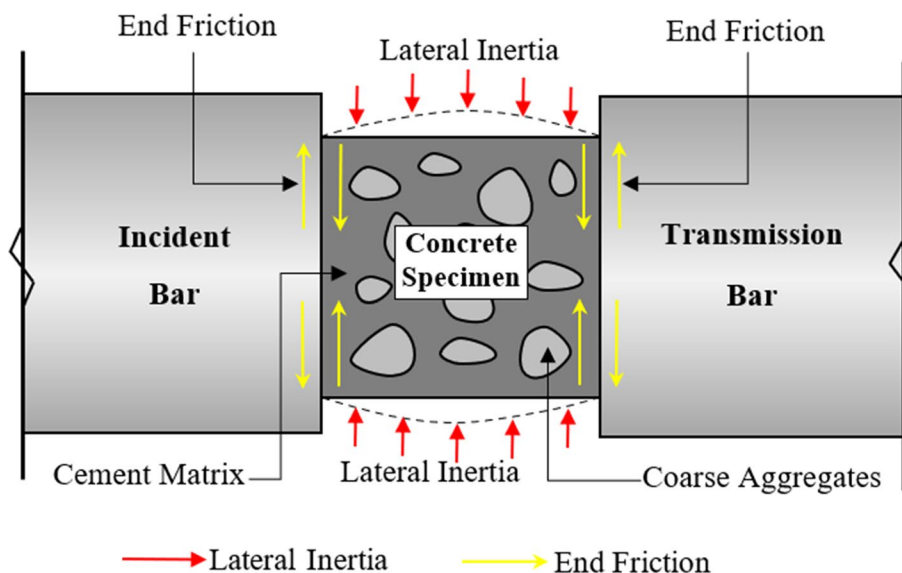
quadratic equation trendline on the curve fitting, see Fig. 5b. The DIF value was found to be increased from 1.16 to 1.78 as the strain rate increases from 72 to 284 s<sup>-1</sup>. A maximum of 1.78 DIF was observed at 284 s<sup>-1</sup> strain rate, describing an 78% strength increment was observed as the loading condition changed from quasi-static to dynamic. A good correlation between DIF and strain rate was observed. The linear and quadratic equations were obtained by the curve fitting method for the compressive strength and DIF, respectively. These equations show good fitting trendlines with the experimental results, and the coefficient of determination (*R*<sup>2</sup>) is more than 0.9.

The increase in strength is primarily influenced by two factors: the material effect and the confinement effect. The material effect is attributed to material heterogeneity, encompassing inherent microstructure and the propagation of cracks in coarse aggregates. Simultaneously, the confinement effect involves lateral inertia and end friction confinement effects [43, 44]. During the static loading, the generated cracks normally propagate along ITZ (interface

transition zone) because there is enough time for the propagation of cracks. On the other hand, under dynamic loading, the generated cracks did not get enough time to propagate through the weaker interface; thus, the crack propagates through the strong coarse particles. It has also been noticed that the delay in the formation of microcracks also contributes to the strength enhancement.

Furthermore, it was noted that the increase in material strength is significantly influenced by both end friction confinement and lateral inertia confinement during dynamic testing. The friction at the interface of the bars and specimen restricts the lateral deformation of the concrete specimen, as illustrated in Fig. 6. Additionally, the specimen experiences lateral deformation due to the Poisson's effect on the concrete material. This lateral deformation results in a backward inertia-induced force, as lateral confinement restricts the lateral deformation, as depicted in Fig. 6. Consequently, the concrete specimen demonstrates an ability to withstand higher lateral deformation through lateral inertia and interface friction confinement, leading to a significant

**Fig. 6** End friction and lateral inertia confinement during high-speed compression test



improvement in dynamic compressive strength and DIF under dynamic compression loading conditions [42, 43].

In the past, many researchers have conducted experimental tests on concrete and concrete-like materials using the SHPB technique. These researchers have proposed various empirical equations based on strain rate to describe the strength increment in terms of DIF [21, 44–48]. These expressions may vary either in logarithmically or polynomial or exponentially with respect to the strain rate. The details of some empirical equations proposed by the researchers for calculating the DIF for concrete, mortar, and concrete-like materials are summarized in Table 2.

The suggested DIF material models and concrete experimental results under high strain rates are shown in Fig. 7. Based on these results, it has been observed that DIF empirical equation obtained by curve fitting method shows an increasing trend as the strain rate increases. Besides, a low increase in the compressive strength has been observed before the transition strain rate, after that a large increase in the strength has been found. The mathematical relationship

obtained through the curve fitting method has been found to be a polynomial equation, which can be as follows;

$$DIF = 2.2569(\log \dot{\epsilon})^2 - 8.718(\log \dot{\epsilon}) + 9.5745 \quad (9)$$

DIF models suggested by Grote et al. [45] and Li and Mang [21] have described underestimation in the results in comparison with the present experimental results, while all available DIF models have been described overestimation in the results in comparison with the present experimental results. This deviation might be due to considering the different analysis methods to develop DIF models, based on their experimental data, experimental conditions, specimen dimension variation, and differences in material strength [47].

### Dynamic stress–strain curve

The dynamic stress–strain curve of the concrete specimen at different strain rates is shown in Fig. 8. These curves are

**Table 2** Dynamic increase factor (DIF) materials model suggested by the researchers

Previous work	Type of material	DIF material model for dynamic compression	Transition strain rate
CEB-FIP 1990 [44]	Concrete-like materials	$DIF = \frac{f_{cd}}{f_{cs}} = \gamma_s \left[ \frac{\dot{\epsilon}}{\dot{\epsilon}_s} \right]^{1/3}$	$\dot{\epsilon} > 30 \text{ s}^{-1}$
Tedesco and Ross 1998 [45]	Concrete	$DIF = 0.758(\log \dot{\epsilon}) + 0.289 \leq 2.5$	$\dot{\epsilon} > 63.1 \text{ s}^{-1}$
Li and Mang 2003 [21]	Mortar	$DIF = 0.03438(\log(\dot{\epsilon}) + 3) + 1.2275$ $DIF = 1.729(\log \dot{\epsilon})^2 - 7.1372(\log \dot{\epsilon}) + 8.5303$	$\dot{\epsilon} \leq 100 \text{ s}^{-1}$ $\dot{\epsilon} > 100 \text{ s}^{-1}$
Zhou and Hao 2008 [46]	Concrete-like materials	$DIF = 0.2713(\log \dot{\epsilon})^2 - 0.3563(\log \dot{\epsilon}) + 1.227$	$\dot{\epsilon} \geq 10 \text{ s}^{-1}$
Grote et al. 2001 [47]	Mortar	$DIF = 0.0235(\log(\dot{\epsilon}) + 1.07$ $DIF = 0.882(\log \dot{\epsilon})^3 - 4.4(\log \dot{\epsilon})^2 + 7.22(\log \dot{\epsilon}) - 2.64$	For $\dot{\epsilon} \leq 266 \text{ s}^{-1}$ For $\dot{\epsilon} > 266 \text{ s}^{-1}$
Katayama et al. 2007 [48]	Concrete	$DIF = 0.2583(\log \dot{\epsilon})^2 - 0.0507(\log \dot{\epsilon}) + 1.021$	–

**Fig. 7** Comparison of experimental results with the existing DIF models in compression

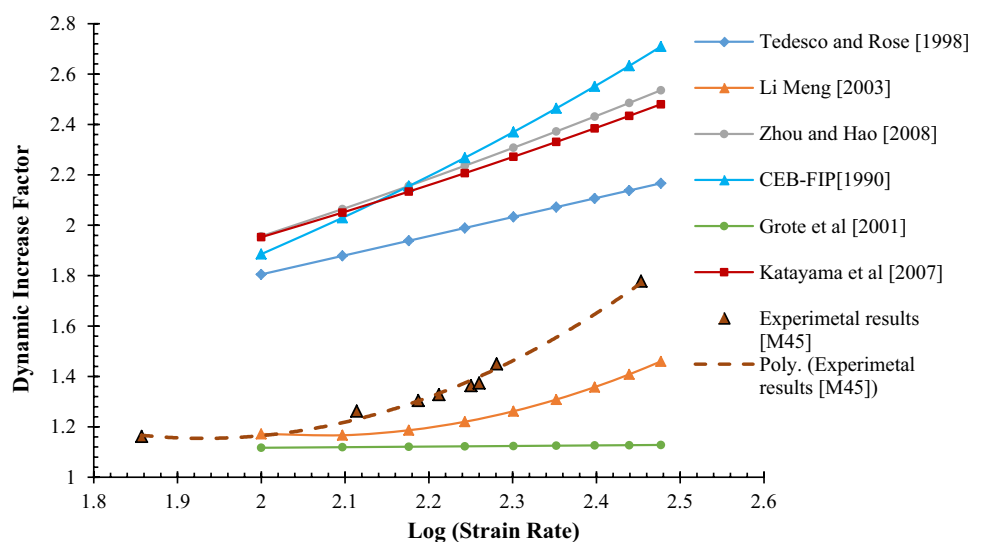
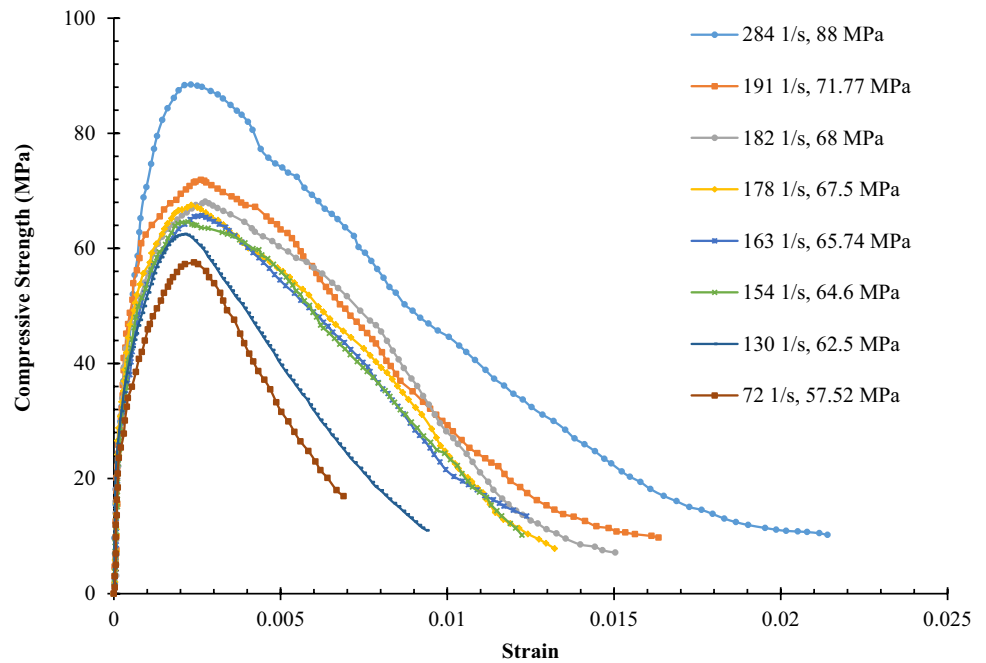


**Fig. 8** Stress–strain curve at different strain rate



obtained with the help of Eqs. (3) and (4) by eliminating the time axis. It has been observed that the dynamic strength increased with strain rate and the curves also appeared to be similar and hence can be utilized to illustrate the strain rate dependency of the dynamic compressive strength. All the specimens showed a nearly linear strength increase trends until reaching peak stress, followed by a flattening softening effect that intensified with higher strain rates. The concrete showed a higher plastic behaviour than the elastic behaviour under high strain rates. The strain corresponding to maximum dynamic compressive strength is also an essential parameter for dynamic material characterization of concrete. It has been observed that strain at peak stress varies in the range of 0.002 to 0.003, but the ultimate strain increases from 0.00689 to 0.0214 as the strain rate increases from 72 to 284 s<sup>-1</sup>. The strain-softening behaviour was observed at a high strain rate, and this behaviour increased with an increase in strain rate. However, the increasing and decreasing of failure strain with strain rate is very small in amount and may be within the range of experimental error and manufacture defect [47].

**Energy absorption density**

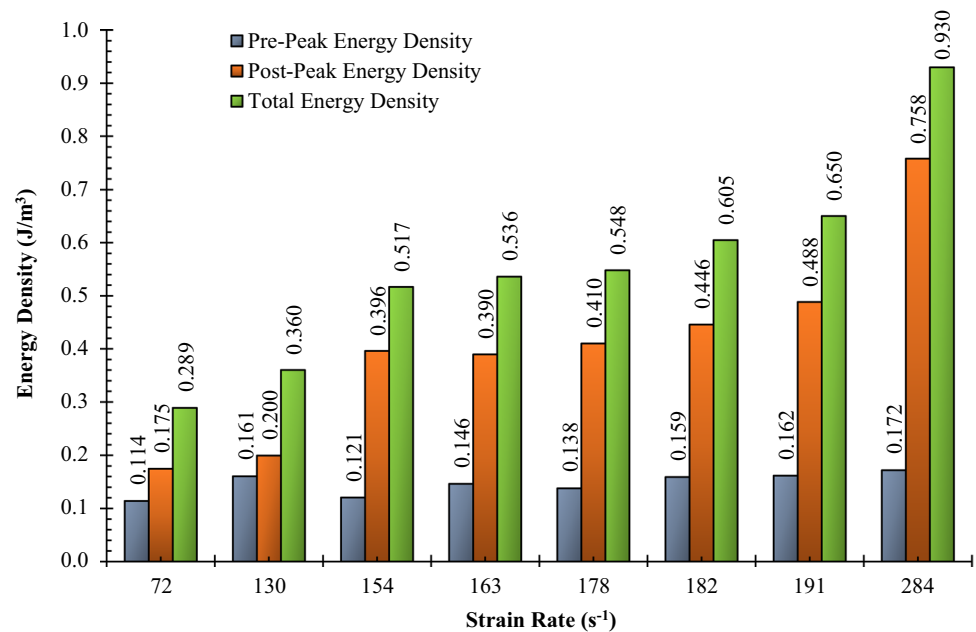
The concrete material's energy absorption capacity refers to the quantity of energy absorbed per unit volume, commonly known as toughness. This also attribute measures the concrete's resistance to fracture or deformation under dynamic or impact loading conditions. Toughness is quantified by calculating the area under the stress–strain curve. In the current study, the energy density is determined

using a straightforward integration method, specifically the trapezoidal rule, as outlined in provided Eq. (10),

$$w = \int \sigma(\epsilon)d\epsilon \tag{10}$$

where *w* is the energy absorption density (toughness),  $\sigma$  is the stress, and  $\epsilon$  is the strain. The energy density corresponding to strain rate is obtained by applying Eq. (10) on stress–strain curve shown in Fig. 8. The toughness of concrete specimens under different strain rates is shown in Fig. 9. The toughness was significantly influenced by strain rate, and increasing trend was observed with increase in strain rate. The toughness increased from 0.289 to 0.930 J/m<sup>3</sup> as the strain rate changed from 72 to 284 s<sup>-1</sup>. An increasing trend of total, pre-peak, and post-peak energy densities was observed with increase in strain rate. There was ~51% increment in the pre-peak energy, but there was ~333% significant increment in the post-peak energy that was observed as the strain rate increases from 72 to 284 s<sup>-1</sup> describing that the higher amount of energy was observed during cracks propagation rather than crack initiations. Furthermore, concrete specimens exhibit increased energy absorption density beyond the peak stress, due to higher strain and strain-softening characteristics. Under the dynamic loading, the developed microcracks required higher energy to propagate through the stiffer particles in the specimen than the energy required to initiate the new crack [50]. Under the high strain rate loading conditions, the concrete is severely damaged, and the failure becomes more severe with continuous increase in the strain rate; hence, the energy absorption capacity increased. The specimen S1-L30-D30 shows the

**Fig. 9** Energy absorption capacity of concrete at different strain rate



lowest dynamic strength and lower toughness as the quantity of micro- and major cracks is less, while the specimen S9-L30-D30 shows higher strength and higher toughness with large numbers of micro- and major cracks at 72 s<sup>-1</sup> and 284 s<sup>-1</sup> strain rate, respectively.

#### Dynamic failure process and crack growth propagation

High-speed photography has been performed at 40,000 frames per second (FPS) to visualize the failure process of the concrete specimen. The images shown in Fig. 10a were captured at six different frames with time interval of 25 microsec to reveal the failure process. It was observed that the specimen failure primarily occurred due to tension developed in the direction perpendicular to the compressive loading which occurred throughout the specimen length starting at the interfaces, see Fig. 10a. An almost similar failure pattern has been observed under the dynamic compression testing. The failure process and deformation of specimen (S2-L30-D45) correspond to 130 s<sup>-1</sup> strain rate under dynamic compressive along with the generated stress–strain graph at the corresponding time of loading shown in Fig. 10b. Under uniaxial loading the specimen stress increased to follow the linear elastic deformation pattern up to point (b) [ $T=25 \mu\text{s}$ ] and reached to nearly 50% of dynamic compressive strength, but as the loading increased, the nature becomes nonlinear elastic up to point (c) [ $T=50 \mu\text{s}$ ]. At  $T=75 \mu\text{s}$ , the microcracks generated at the interface of specimen and bar appeared, showing that the specimen has reached its maximum load-carrying capacity and strength started to decreased beyond the peak stress up to the point (d), see Fig. 10b. The number of cracks

initiated at the interface increased during the loading time of 75–100  $\mu\text{s}$  and progressed into major cracks leading to failure of concrete specimen, which further reduced the strength up to point (e), see Fig. 10b. As the loading time increased beyond the 100  $\mu\text{s}$  the major cracks further penetrated the concrete matrix and caused the failure of the specimen with permanent deformation at  $T=125 \mu\text{s}$ , see Fig. 10a. Many microcracks were observed beyond the 100- $\mu\text{s}$  loading time with decrease in the concrete strength, but the deformation increased. It also observed that the strain-softening behaviour increased with an increase in strain rate as the deformation increases beyond the peak strain in Fig. 8.

#### Failure mode and fragmentation

The researchers [25, 26, 47] noticed that the specimen was completely crushed into fragments, but the size and quantity of the fragments varied significantly depending on the strain rate. The fragments of tested specimens S1-L30-D30 and S8-L30-D30 recovered from a high-speed SHPB compression test conducted at both low and high strain rates illustrated in Fig. 11. It was observed that the strain rate had a significant impact on the failure pattern and fragmentation of the concrete specimens. At low strain rate of 72 s<sup>-1</sup>, it was observed that the specimen failed with typically bigger pieces of fragments with small crushed amount of concrete, see Fig. 11a, while at high strain rate of 284 s<sup>-1</sup>, the concrete specimen completely damaged and catastrophically scattered into small size fragments with higher crushing amount of concrete, see Fig. 11b.

A total of 13, 43, 53, and 79 fragments were recovered having the size larger than 4.75 mm at 72, 163, 191, and

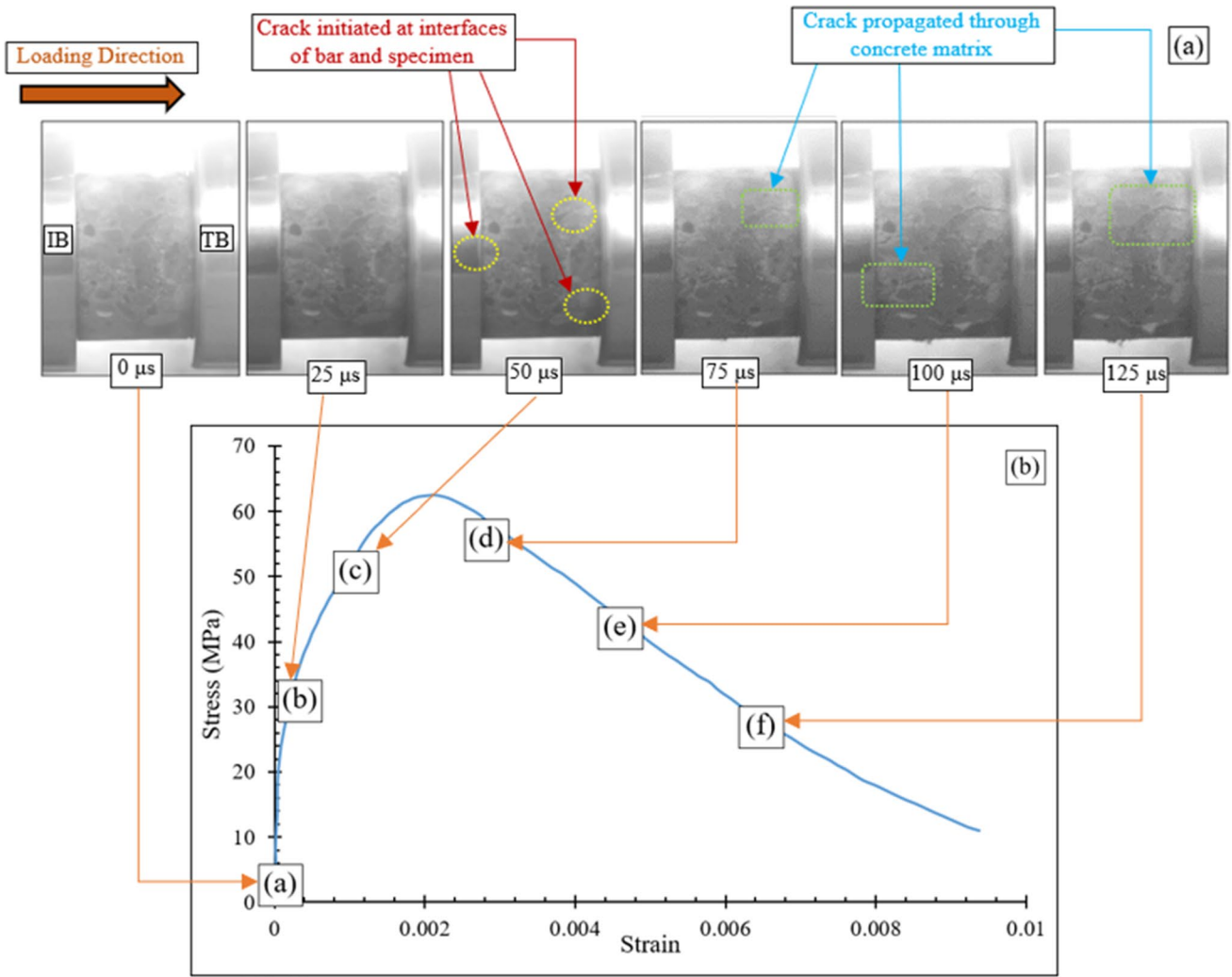


Fig. 10 Behaviour of concrete specimen at 130 s<sup>-1</sup> a failure process, b stress–strain response

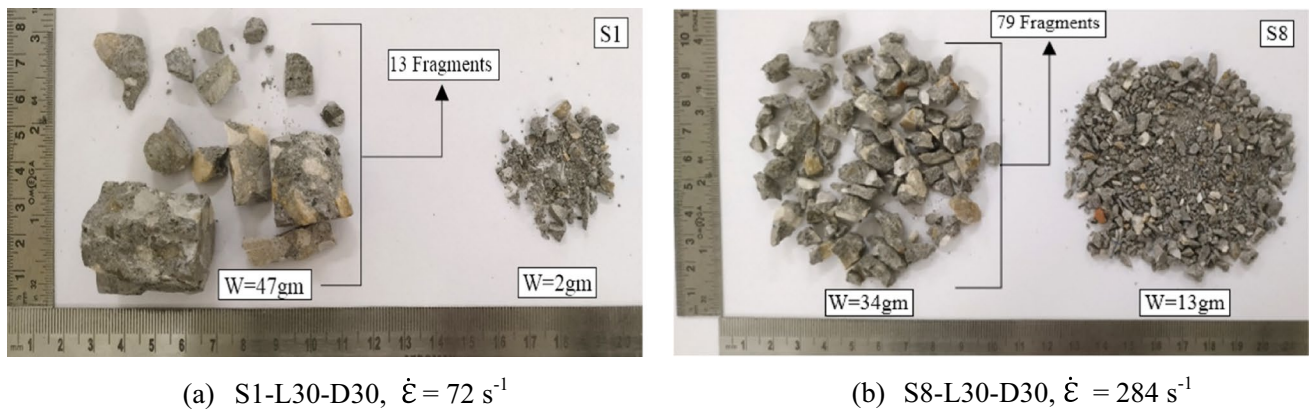


Fig. 11 The tested specimen passed through 4.75-mm sieve

284 s<sup>-1</sup> strain rate for L30-D30 sized specimens, respectively. Similarly, for the L30-D45 sized specimens, a total 130, 178, and 184 fragments were formed at 130, 178, and 182 s<sup>-1</sup> strain rates, respectively. The higher quantity of fragments generated at the higher strain rate for a given size of specimen and showed a similar failure pattern and fragmentation behaviour [25, 26, 47]. In addition, it also observed that the flaky, angular, and uneven shape fragments were formed in all tested concrete specimen, but the number of flaky shape fragments was low at low strain rate test and high at relatively higher strain rate test. As such in most of the cases the shape of the fragments was irregular, and their size decreased with an increase in strain rate. It also found that under high strain rate, a complete failure of the concrete specimen occurred with a larger number of microcracks and the fragments.

The weighing analysis was performed on the tested concrete specimen to examine the crushing density of concrete. This involved sieved the tested specimens through a standard 4.75-mm sieve to separate the coarse and fine particle fragments. It was observed that the percentage weight of concrete specimens (crushed concrete) passed through the 4.75-mm sieve increases with the increase in strain rate, while the retained percentage weight of concrete decreases with increase in the strain rate. The percentage weight of fine fragments increases from 4.08 to 27.66%, while the weight of coarse fragments decreases from 95.925 to 72.34% with an increase in the strain rate from 72 to 284 s<sup>-1</sup>. Hence, it has been concluded that the crushing of concrete increases as the strain rate increases, describing that the concrete crushing is higher at higher strain rate [51].

## Dynamic splitting tensile behaviour of concrete

### Strain rate effect on dynamic tensile strength and DIF

In this current investigation, dynamic splitting tensile strength is characterized as the maximum stress observed in the specimen throughout the loading process, and it is directly proportional to the corresponding peak strain of the transmitted wave. The dynamic tensile properties of concrete specimens satisfying the equilibrium conditions corresponding to their strain rates are listed in Table 3. The dynamic splitting tensile strength, strain rate, and loading rate were determined by using Eqs. (6), (7), and (8), respectively. Like the dynamic compressive strength, the dynamic tensile strength is also significantly increased with an increase in the strain rate, see Fig. 12a. It was observed that the dynamic tensile strength increases from 12.76 to 21.89 MPa as the strain rate increases from 6.79 to 14.95 s<sup>-1</sup>. There was 303.87% increment in tensile strength was observed as the strain rate increased from  $6.67 \times 10^{-4}$  to 14.95 s<sup>-1</sup> (quasi-static to dynamic loading condition). Hence, the splitting

**Table 3** Dynamic tensile properties at high strain rate

Length	Diameter	Strain rate	Loading rate	Dynamic tensile strength (Ftd)	DIF
mm	mm	(1/s)	(MPa/s)	(MPa)	(Ftd/Fts)
31.2	30	6.79	227,839.66	12.76	2.35
30.1	30	5.86	196,594.67	13.37	2.47
29.7	30	6.39	214,321.49	13.50	2.38
31.0	30	7.62	255,700.91	13.58	2.49
31.2	30	8.83	296,125.51	15.10	2.78
30.7	30	10.19	341,753.10	17.49	3.22
30.9	30	10.70	358,982.38	18.31	3.38
31.5	30	12.10	405,986.30	19.08	3.52
30.5	30	14.95	501,426.62	21.89	4.04

tensile strength clearly showed the higher sensitivity to the strain rate as compared to compressive strength.

The DIF is generally used to describe the higher strain rate effect on material properties quantitatively. DIF of tensile strength was obtained as the ratio of dynamic tensile strength normalized with the quasi-static tensile strength 5.42 MPa and the relationship of DIF with strain rate shown in Fig. 12b. All the DIF were greater than one describing that the dynamic tensile strength is higher than the quasi-static strength. The minimum and maximum DIF values were obtained as 2.35 and 4.04 corresponding to 6.79 and 14.95 s<sup>-1</sup> strain rate, respectively. A nearly ~72% DIF increment was observed as the loading rate increased from 227.83 to 501.42 GPa/s. The increasing trends of DIF with strain rate are clearly observed in Fig. 12b. The best fitting curve method was used for strong relation between strength and strain rate. In Fig. 12a, it was observed that the dynamic tensile strength is linearly correlated with the strain rate (see Fig. 12a), but the DIF showed a polynomial correlation with the logarithmic strain rate, see Fig. 12b. Hence, based on result output it was concluded that the dynamic tensile strength and DIF showed a strong increasing correlation with increase in strain rate. The trendlines obtained through curve fitting method showed the higher acceptability of results with a coefficient of determination ( $R^2$ ) more than 0.90 and described the strong relation.

The possible explanation of strain rate effects on dynamic splitting tensile strength enhancement includes the following main aspects: (1) evaluation and propagation of cracks (see, Fig. 13a) and (2) inertia effect (see Fig. 13b). It has been noticed that the transgranular propagation of crack occurred under dynamic splitting tensile test and the generated cracks propagate through the strong coarse particle have higher stiffness (coarse aggregates), which is one of the main reasons behind increase in the tensile strength of the concrete material, see Fig. 13a. Additionally, the specimen

**Fig. 12** Tensile behaviour of concrete **a** tensile strength–strain rate, **b** tensile DIF–log (strain rate)

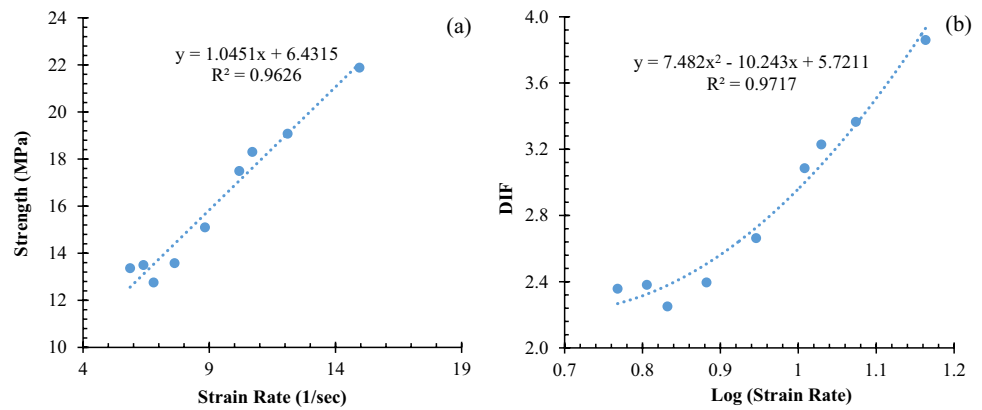
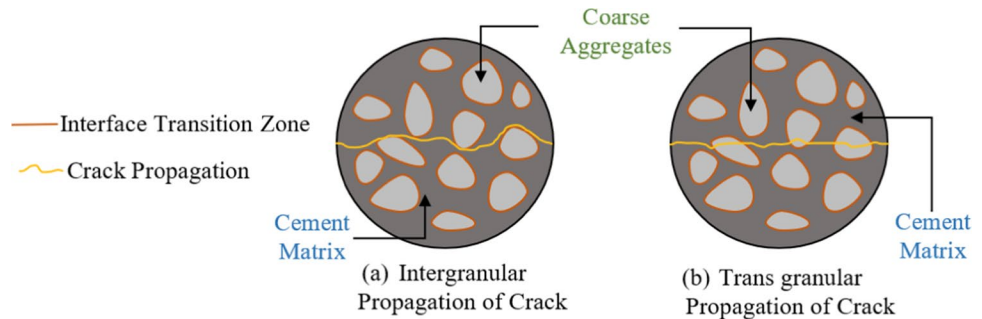
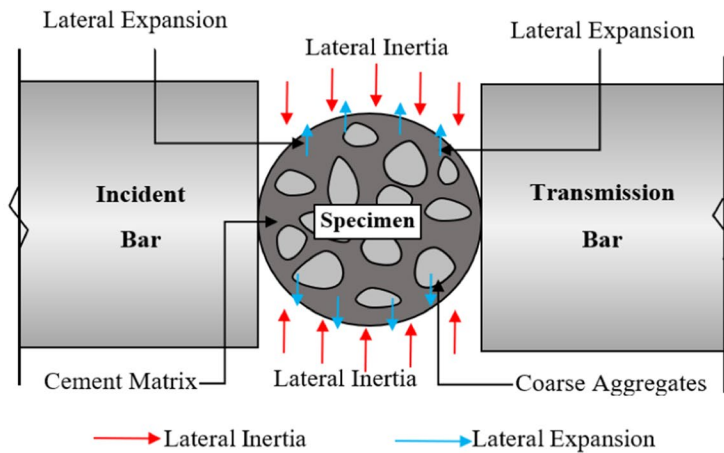


**Fig. 13** Dynamic response of concrete under tension **a** crack propagation, **b** lateral inertia confinement



(a) Propagation of Crack under quasi-static and dynamic loading condition



(b) Lateral inertia confinement during high-speed tensile test

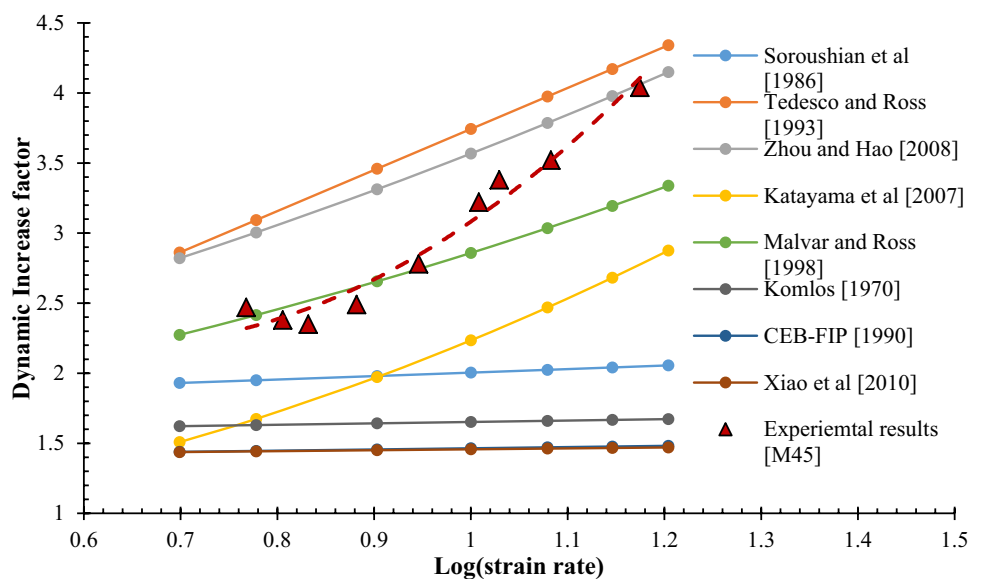
experienced the lateral deformation due to Poisson’s ratio of concrete material. This lateral deformation results in a backward inertia-induced force as lateral confinement limits the lateral deformation, which further increased the tensile strength of concrete. Hence, this inertia effect also contributed to strength enhancement under high strain rate loading conditions due to inertial force generated in concrete specimen (see Fig. 13a) [51, 52].

In the last few decades, many researchers have been performing the large numbers of experiments on concrete and concrete like brittle materials to investigate the strain rate effects on the dynamic tensile strength. Based on experimental and numerical study, the researchers proposed the DIF material model to predict the dynamic behaviour of brittle materials in tension. Some of the suggested models are summarized in Table 4 for performing the comparative study.

**Table 4** Dynamic increase factor (DIF) materials model suggested by various researchers

Previous work	Material type	DIF material model for tension	Transition strain rate
Tedesco and Ross 1993 [14]	Concrete	$DIF = 0.1425[(\log \dot{\epsilon}) + 5.8456] + 1 \leq 6.0$	$\dot{\epsilon} > 2.32 \text{ s}^{-1}$
Malvar and Ross 1998 [18]	Concrete	$DIF = \gamma_s \left[ \frac{\dot{\epsilon}}{\dot{\epsilon}_s} \right]^{1/3}$	$\dot{\epsilon} > 1 \text{ s}^{-1}$
CEB-FIP 1990 [44]	Concrete-like materials	$DIF = \left[ \frac{\dot{\epsilon}}{\dot{\epsilon}_s} \right]^{1.016\alpha_s}$	$\dot{\epsilon}_s < \dot{\epsilon} \leq 30 \text{ s}^{-1}$
Zhou and Hao 2008 [46]	Concrete-like materials	$DIF = 0.7325(\log \dot{\epsilon})^2 + 1.235(\log \dot{\epsilon}) + 1.6$	$\dot{\epsilon} > 0.1 \text{ s}^{-1}$
Katayama et al. 2007 [48]	Concrete	$DIF = 1.4379(\log \dot{\epsilon})^2 - 0.02987(\log \dot{\epsilon}) + 0.8267$	–
Soroushian et al. 1986 [53]	Concrete	$DIF = 0.0154(\log \dot{\epsilon})^2 + 0.219(\log \dot{\epsilon}) + 1.77$	–
Komlos 1970 [54]	Concrete	$DIF = 1.0 + 0.11 \log \left[ \frac{\dot{\epsilon}}{\dot{\epsilon}_s} \right]$	–
Xiao et al. 2010 [55]	Concrete	$DIF = 1 + 0.0653 \log \left[ \frac{\dot{\epsilon}}{\dot{\epsilon}_s} \right]$	–

**Fig. 14** Comparison of experimental results with the existing DIF models in tension



In Fig. 14, the experimental results were compared with the suggested DIF model for concrete in tension. It was found that all DIF empirical relations follow a similar trend, that is, DIF increases with the strain rate. While the empirical relationship obtained through the curve fitting method, based on the experimental results, was found to be quadratic, it can be described as

$$DIF = 7.482(\log \dot{\epsilon})^2 - 10.243(\log \dot{\epsilon}) + 5.7211 \quad (10)$$

The experimentally developed DIF curve shows a good agreement with the DIF models suggested by the [14, 18, 46]. The DIF empirical models suggested by various researchers agree well with their respective experimental data but need to be consistent with the experimental data obtained by other researchers. This inconsistency might be

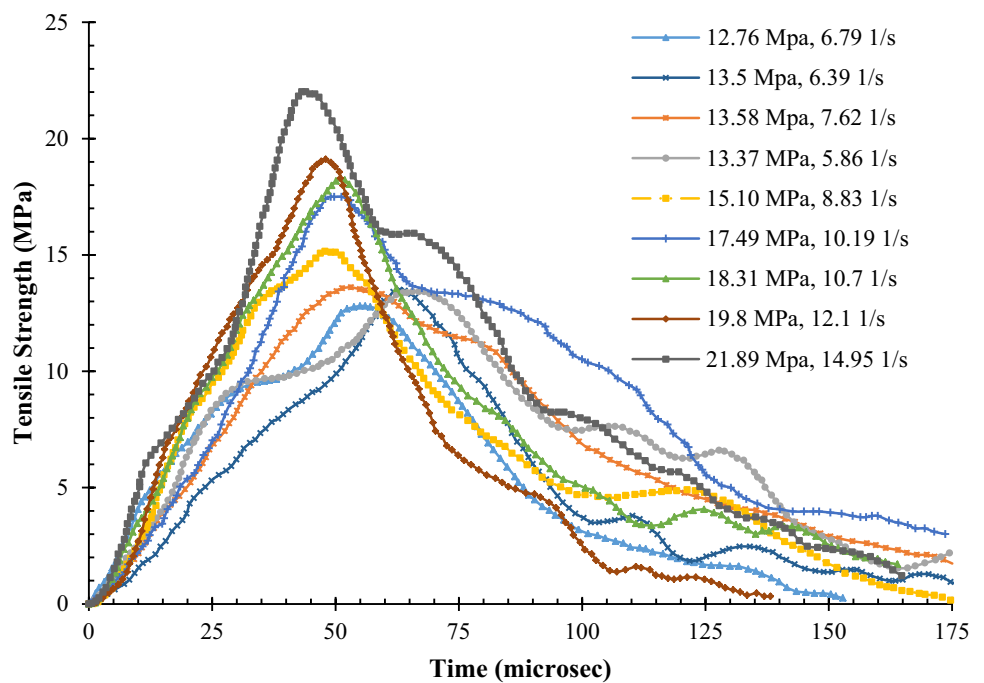
due to differences in the material strength and their constituents, specimen dimensions, and loading condition.

**Strength–time response**

The tensile strength and time response of concrete under different strain rates is shown in Fig. 15. It was observed that the tensile strength is generally inversely proportional to the loading time and increases with a decrease in loading duration. The strength–time curves showed a similar profile, but the peak strength amplitude increases with increase in loading rate. Under high impact velocity, the loading duration on concrete specimen is too much shorter and concrete reaches to its peak strength very soon. It has been noticed that, as the loading duration decreases from 68 to 43.9 microsecond, the loading rate increases from 196.59 to 501.42 GPa/s and strain rate increases from 5.86 to 14.94 s<sup>-1</sup>. In other



**Fig. 15** Strength–time response at different strain rate



words, as the loading duration is shorter, the tensile strength is higher. Hence, it has been concluded that as the loading duration increases, the tensile strength approaches the quasi-static value. During a shorter loading time, there are many microcracks triggered, but there is no delay for already triggered cracks to propagate the relatively larger distance towards the loading ends. Hence the large number of small cracks was the main cause for higher tensile strength under short loading duration [17].

**Quasi-static and dynamic fracture surface**

The fracture surface of concrete specimen under quasi-static splitting tensile test and dynamic splitting tensile test is shown in Fig. 16. The dynamic failure mode of concrete is completely different from the quasi-static failure mode in terms of crack propagation behaviour. Under high strain rate loading, the transgranular propagation of cracks phenomenon occurred, while under quasi-static loading conditions, the intergranular propagation of cracks occurred [25–27]. The failure crack orientation is axial and parallel to the loading direction which splits the specimen into two pieces. In quasi-static loading conditions, the initiated cracks have sufficient time to propagate through the weaker ITZ or other areas with lower resistance. They do not penetrate through strong aggregates due to their high strength, resulting in a rough failure surface, see Fig. 16a. In high strain rate loading tests the loading duration is very short, and cracks do not get enough time to propagate through weaker sections. Hence, the initiated microcracks propagate more rapidly and quickly through coarse aggregates rather than the interfacial

transition zone (ITZ), see Fig. 16b. Thus, the coarse aggregates particle is broken during the high strain rate and the fracture surface was smooth and flatter, see Fig. 16b. A similar trend of concrete fracture surface is also reported by the other researchers [8, 15, 20].

**Fracture process and crack growth propagation**

In the dynamic splitting tensile test, the experimental validity and acceptability of the results were investigated through following aspects: (1) stress equilibrium condition:—the concrete specimen must be in equilibrium conditions during the tensile test, (2) first crack initiation location:—it is necessary to check the location of initiation of the first crack in concrete specimen, whether the failure crack initiated from the centre point of the specimen, and (iii) propagation of crack:—it is also important to track the route of crack propagation path such that the failure path should be almost parallel to the loading direction [15]. A high-speed video camera is used to monitor the fracturing process of the cylindrical specimen under dynamic loading conditions. The camera has been placed perpendicular to the sample surface recorded at 40,000 frame per second (*fps*). The crack initiation and propagation in cylindrical specimen recorded at 7.62 s<sup>-1</sup> strain rate is shown in Fig. 17a. At *T*=0 μs, the tensile strength is zero and loading started in the specimen. During the lading time between *T*=0 and *T*=50 μs, load-carrying capacity of concrete increases and no crack was observed at the centre of specimen. At *T*=75 μs, the primary crack was observed at the centre of the specimen. Hence during the *T*=50 to *T*=75-μs loading time, the stress at the

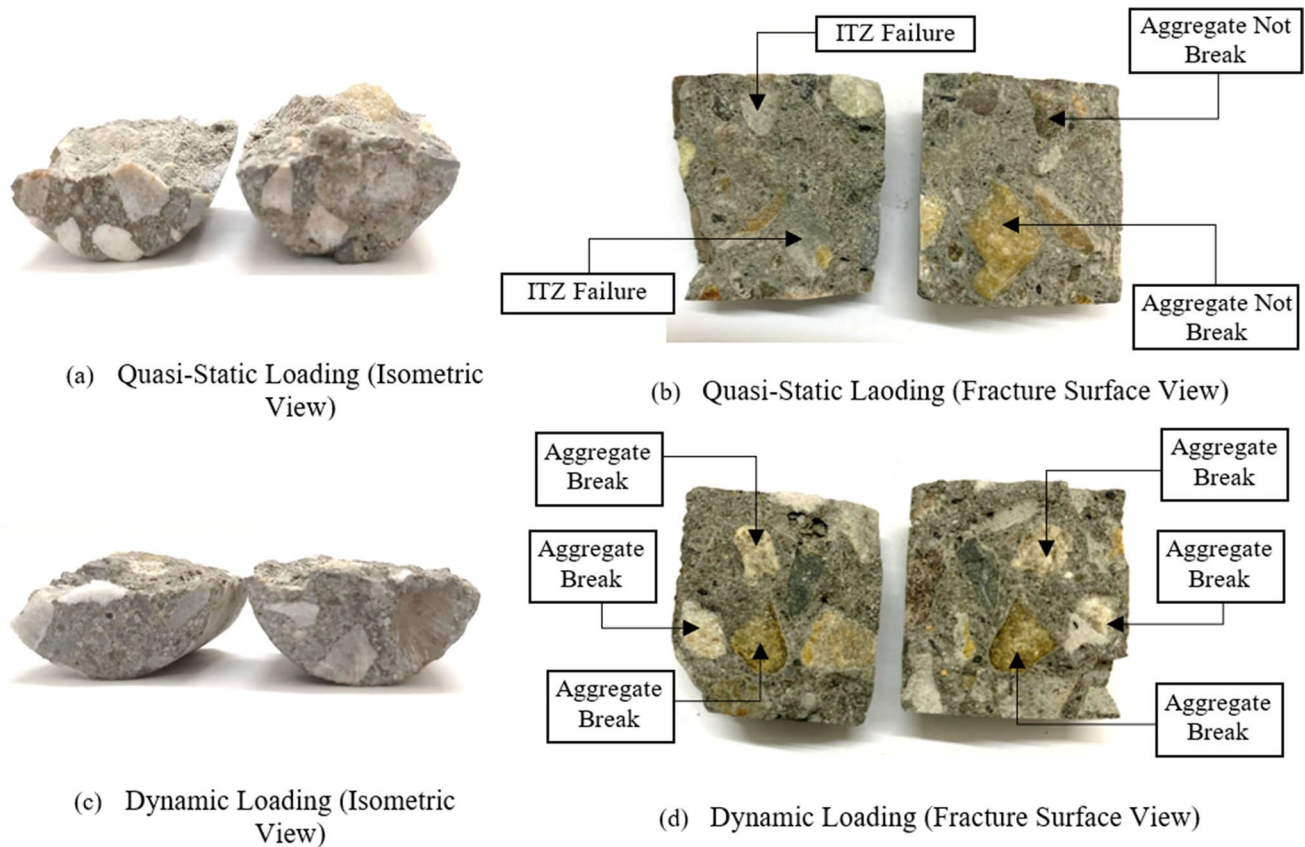


**Fig. 16** Failure surfaces **a** quasi-static failure surface, **b** dynamic failure surface

specimen and bar interface reached to the equilibrium conditions and the maximum tensile stress occurred at the centre of the specimen. This concludes that the splitting of the cylindrical specimen takes place at the centre and validates the working principal of splitting tensile test under dynamic loading [17]. At around  $T = 100 \mu\text{s}$ , it was also observed that the first initiated crack quickly propagated towards the loading ends and crack direction was almost parallel to the loading direction, see Fig. 17a. When the crack reached to the end interfaces at  $T = 125 \mu\text{s}$ , the concrete specimen split in to two semi-cylindrical parts and failure occurred through splitting tensile phenomena, see Fig. 17a. The further increase in loading on the concrete specimen starts to crush the concrete at the loading end interfaces beyond the time  $T = 125 \mu\text{s}$ .

#### Failure process corresponding to strength–time response

The failure process and strength–time response of concrete specimen at the  $7.62 \text{ s}^{-1}$  strain rate with their corresponding time of loading is illustrated in Fig. 17b. The load starts to increase from zero corresponding to point (a). The concrete dynamic splitting tensile strength increased from point (a) up to the point (c) and the concrete remained in linear

elastic region as there was no crack was observed at centre of specimen, Fig. 17a. Between the point (c) and (d) in the strength–time response curve in Fig. 17b, concrete reaches its maximum tensile strength just before it starts to weaken beyond the point of failure. Beyond the point (d), the tensile strength reduces, and strength tends to zero corresponding to the point (f). The concrete specimen split into two semi-cylindrical halves, exhibiting similar tensile crack initiation, propagation, and splitting tensile behaviour as reported in the literature [17].

#### Failure mode and fragmentation

The failure pattern of tested specimen is an important indicator to understand strain rate effect on the failure mode of concrete specimen under dynamic splitting tensile tested at different high strain rates as shown schematically in Fig. 18a. It has been observed that all the cylindrical specimens followed an almost similar mode of failure of splitting in to two semi-cylindrical halves. In addition, the contacts area between specimen and bars appeared to be local crushing as the strain rate increases. At low strain rate, the specimen split into semi-cylindrical halves with or without small wedge regions, but under high strain rate the large wedge

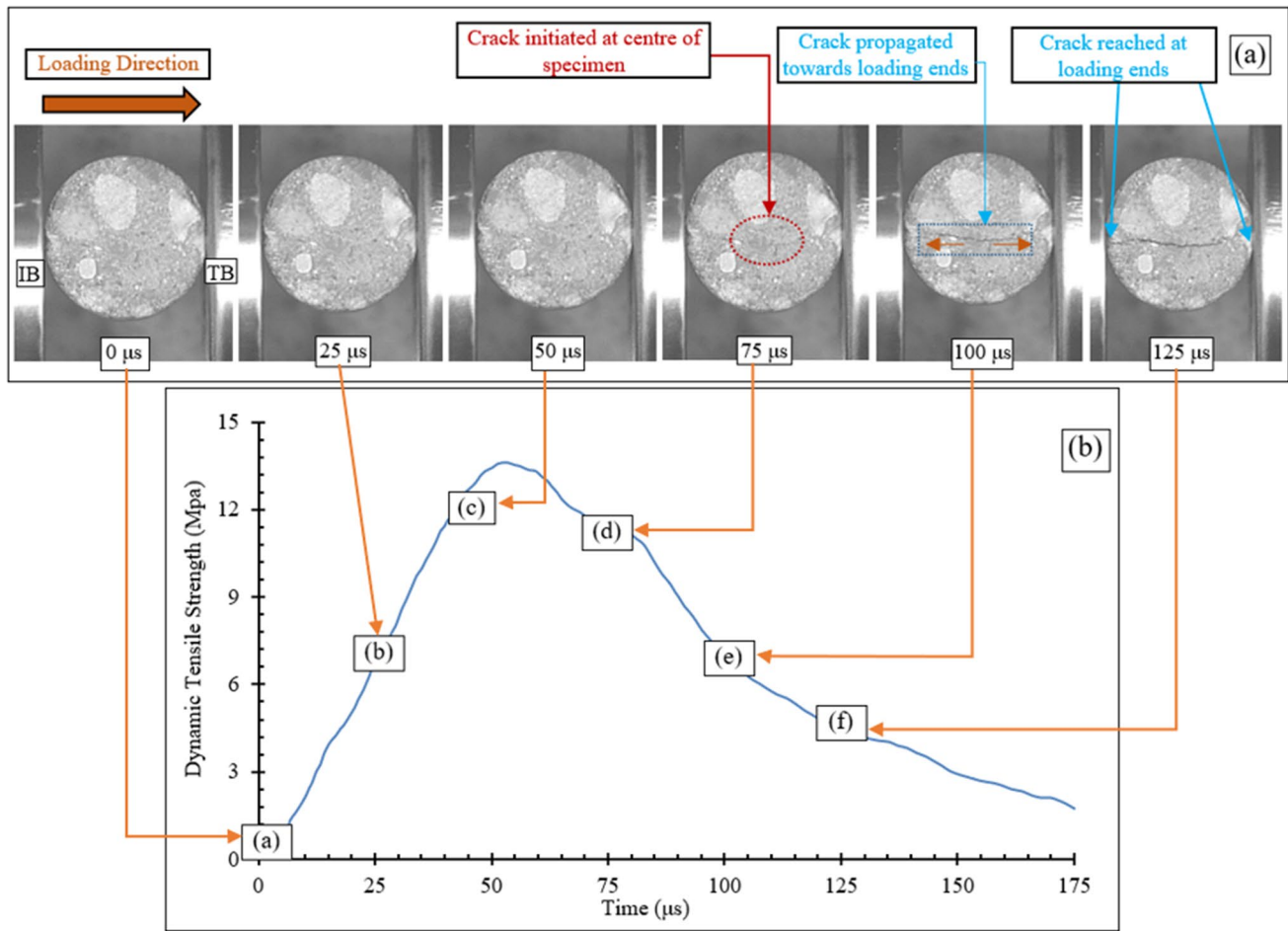


**Fig. 17** Dynamic splitting tensile test at  $7.62 \text{ s}^{-1}$  strain rate **a** failure process, **b** strength–time response

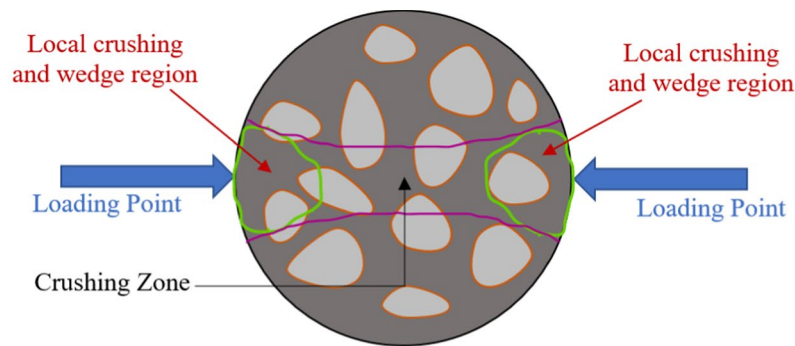
region was formed and large crushing of concrete occurred at the loading contact points as shown in Fig. 18a, while at very high strain rate, in addition to large wedge region, the crushing zone was also formed along the loading direction. Hence, it has been concluded that the loading rate plays an important role in the concrete failure mode pattern under dynamic loading conditions. Moreover, with increase in strain rate, the crushing of concrete increases at the loading ends and the wedged shape formed at the concrete failure edges also increases, see Fig. 18a [15]. The main major macro-crack develops at the centre of disc, but other cracks also develop at the contact points due to high loading which crushed the concrete specimens into small fragments as shown in Fig. 18b. At  $5.86 \text{ s}^{-1}$ , the failure in the concrete specimen takes place in such a way that it splits into two almost equal pieces with small crushing of about 2 gm, while, at  $10.7 \text{ s}^{-1}$  strain rate, the specimen splits into two major pieces with concrete crushing of about 7 gm leading to developing a crushing zone along the loading direction. In terms of energy, the wave propagates in bar associates with the energy. At the low loading rate, the energy associated

with the incident wave was so small, for that reason the energy absorbed by the specimen was primarily used initiation and generation of main crack and split the specimen into two complete parts with very small amount of crushed concrete at the contact points. Under higher loading rate, the incident energy associates with incident were very high and the part of energy used for initiation and propagation of generated main crack, while the remaining energy was used to crush the concrete specimen at the contact area between specimen and bars [29].

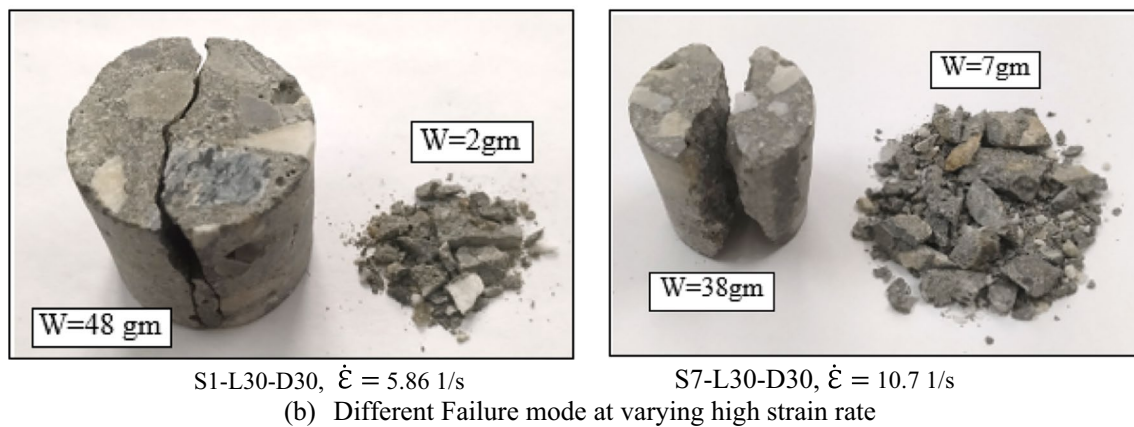
### Conclusion

The following outcomes have been observed for dynamic compression and splitting tensile test:

- The dynamic compressive strength of concrete increases from 57.5 to 88 MPa with an increase in the strain rate from 72 to  $284 \text{ s}^{-1}$  describing the strain rate sensitivity of the concrete.



(a) Specimen failure under dynamic loading conditions



(b) Different Failure mode at varying high strain rate

**Fig. 18** **a** Failure mechanism, **b** failure mode of concrete specimen

- The energy absorption capacity significantly increased from 0.289 to 0.930 J/m<sup>3</sup> as the strain rate increased from 72 to 284 s<sup>-1</sup> due to the formation of large number of cracks and confinement effects. Notably, concrete's plastic behaviour exhibited greater sensitivity to high loading rates compared to its elastic behaviour.
- The strain rate was significantly affected by the concrete damage describing that the percentage weight of crushed specimen passing through the 4.75-mm sieve was increased from 4.08 to 27.66% with an increase in strain rate from 72 to 284 s<sup>-1</sup>.
- The damaged concrete fragments retained by a 4.75-mm sieve were flaky, angular, and irregular in shape. Their number increased as the strain rate increased, leading to smaller fragment sizes.
- The dynamic splitting tensile strength of concrete found to be more sensitive to strain rate and increases from 12.76 to 21.89 MPa as the strain rate increases from 6.79 to 14.95 s<sup>-1</sup> due to the transgranular propagation of the cracks.
- The failure pattern in dynamic tension significantly depends upon the strain rate. The tested specimen split

into two semi-cylindrical pieces at low strain rate, while at high strain rate, the local crushing was initially happened in the specimen which leading to developing the crushing zone (wedge region) in the concrete specimen due to increase in the rate of loading.

- The experimental results revealed a DIF of 1.78 at a strain rate of 284 s<sup>-1</sup> for compression and a DIF of 4.04 at a strain rate of 14.95 s<sup>-1</sup> for tension. This indicates that concrete exhibits greater sensitivity to dynamic tension compared to dynamic compression.

**Acknowledgements** The authors gratefully acknowledge the financial support provided by AERB through the project no. AERB/CSRP/73/03R/2019 for carrying out the present study.

### Declarations

**Conflict of interest** The authors declare that there is no conflict of interest and it is approved by all authors for publication.

**Ethical approval** Our article does not contain any studies with human participants or animals performed by any of the authors.

**Informed consent** Formal consent is not required for this type of study.

## References

- Chen Z, Fang H, Zhu L, Mao Y, Liu W (2020) Experimental tests and numerical simulations of circular reinforced concrete piers under ship impact. *Adv Bridge Eng* 1(1):1–25. <https://doi.org/10.1016/j.ijimpeng.2018.11.016>
- Yoo DY, Banthia N (2017) Mechanical and structural behaviors of ultra-high-performance fiber-reinforced concrete subjected to impact and blast. *Constr Build Mater* 149:416–431. <https://doi.org/10.1016/j.conbuildmat.2017.05.136>
- Jiricek P, Foglar M (2015) Numerical simulation of the effect of regular and sub-caliber projectiles on military bunkers. In: EPJ web of conferences, vol 94. EDP Sciences, p 04049. <https://doi.org/10.1051/epjconf/20159404049>
- Do TV, Pham TM, Hao H (2019) Impact force profile and failure classification of reinforced concrete bridge columns against vehicle impact. *Eng Struct* 183:443–458. <https://doi.org/10.1016/j.engstruct.2019.01.040>
- Qiao PZ, Fan W (2014) Identifying damage in honeycomb fiber-reinforced polymer (FRP) composite sandwich bridge decks. In: *Advanced composites in bridge construction and repair*. Woodhead Publishing, pp. 94–116. <https://doi.org/10.1533/9780857097019.1.94>
- Wang W, Morgenthal G, Helmrich M (2020) Damage identification of a single RC column subjected to barge impact based on optimization strategies. *Ocean Eng* 216:107979. <https://doi.org/10.1016/j.oceaneng.2020.107979>
- Wang W, Wang X, Fu J, Lu Z, Zhou R, Shao Y, et al (2023) A novel frame-type crashworthy device for protecting bridge piers from vehicle collisions. In: *Structures*, vol 57. Elsevier, p 105313. <https://doi.org/10.1016/j.istruc.2023.105313>
- Bischoff PH, Perry SH (1991) Compressive behaviour of concrete at high strain rates. *Mater Struct* 24:425–450. <https://doi.org/10.1007/BF02472016>
- Rizwanullah, Sharma HK (2022) Blast loading effects on UHP-FRC structural elements: a review. *Innovat Infrastruct Solut* 7(6):341. <https://doi.org/10.1007/s41062-022-00937-2>
- Pajak M (2011) The influence of the strain rate on the strength of concrete taking into account the experimental techniques
- Chen WW, Song B (2010) *Split Hopkinson (Kolsky) bar: design, testing and applications*. Springer, Berlin
- ASTM International Committee C09 on Concrete and Concrete Aggregates (2017) *Standard Test Method for Splitting Tensile Strength of Cylindrical Concrete Specimens*. ASTM international
- Barton N (1978) Suggested methods for the quantitative description of discontinuities in rock masses. *ISRM Int J Rock Mech Min Sci Geomech Abstracts* 15(6):319–368
- Tedesco JW, Ross CA (1993) Experimental and numerical analysis of high strain rate splitting-tensile tests. *Mater J* 90(2):162–169. <https://doi.org/10.14359/4013>
- Chen X, Ge L, Zhou J, Wu S (2017) Dynamic Brazilian test of concrete using split Hopkinson pressure bar. *Mater Struct* 50(1):1–15. <https://doi.org/10.1617/s11527-016-0885-6>
- Zhou Z, Li X, Zou Y, Jiang Y, Li G (2014) Dynamic Brazilian tests of granite under coupled static and dynamic loads. *Rock Mech Rock Eng* 47(2):495–505. <https://doi.org/10.1007/s00603-013-0441-4>
- Wang QZ, Li W, Xie HP (2009) Dynamic split tensile test of flattened Brazilian disc of rock with SHPB setup. *Mech Mater* 41(3):252–260. <https://doi.org/10.1016/j.mechmat.2008.10.004>
- Malvar LJ, Ross CA (1998) Review of strain rate effects for concrete in tension. *ACI Mater J* 95:735–739
- Riisgaard B, Ngo T, Mendis P, Georgakis CT, Stang H (2007) Dynamic increase factors for high performance concrete in compression using split Hopkinson pressure bar. In: 6th international conference on fracture mechanics of concrete and concrete structures, pp 1–3
- Brara A, Klepaczko JR (2006) Experimental characterization of concrete in dynamic tension. *Mech Mater* 38(3):253–267. <https://doi.org/10.1016/j.mechmat.2005.06.004>
- Li QM, Meng H (2003) About the dynamic strength enhancement of concrete-like materials in a split Hopkinson pressure bar test. *Int J Solids Struct* 40(2):343–360. [https://doi.org/10.1016/S0020-7683\(02\)00526-7](https://doi.org/10.1016/S0020-7683(02)00526-7)
- Le Nard H, Bailly P (2000) Dynamic behaviour of concrete: the structural effects on compressive strength increase. *Mech Cohes Frict Mater Int J Exp Model Comput Mater Struct* 5(6):491–510. [https://doi.org/10.1002/1099-1484\(200008\)5:6%3c491::AID-CFM106%3e3.0.CO;2-R](https://doi.org/10.1002/1099-1484(200008)5:6%3c491::AID-CFM106%3e3.0.CO;2-R)
- Cotsovos DM, Pavlović MN (2008) Numerical investigation of concrete subjected to compressive impact loading. Part 1: a fundamental explanation for the apparent strength gain at high loading rates. *Comput Struct* 86(12):145–163. <https://doi.org/10.1016/j.compstruc.2007.05.014>
- Tang T, Malvern LE, Jenkins DA (1992) Rate effects in uniaxial dynamic compression of concrete. *J Eng Mech* 118(1):108–124. [https://doi.org/10.1061/\(ASCE\)0733-9399\(1992\)118:1\(108\)](https://doi.org/10.1061/(ASCE)0733-9399(1992)118:1(108))
- Al-Salloum Y, Almusallam T, Ibrahim SM, Abbas H, Alsayed S (2015) Rate dependent behavior and modeling of concrete based on SHPB experiments. *Cement Concr Compos* 55:34–44. <https://doi.org/10.1016/j.cemconcomp.2014.07.011>
- Chen X, Wu S, Zhou J (2013) Experimental and modeling study of dynamic mechanical properties of cement paste, mortar, and concrete. *Constr Build Mater* 47:419–430. <https://doi.org/10.1016/j.conbuildmat.2013.05.063>
- Shemirani AB, Naghdabadi R, Ashrafi MJ (2016) Experimental and numerical study on choosing proper pulse shapers for testing concrete specimens by split Hopkinson pressure bar apparatus. *Constr Build Mater* 125:326–336. <https://doi.org/10.1016/j.conbuildmat.2016.08.045>
- Cai Y, Ren HQ, Long ZL, Guo RQ, Du KM, Chen SS, Zheng ZH (2022) Comparison study on the impact compression mechanical properties of coral aggregate concrete and ordinary Portland concrete. In: *Structures*, vol 44. Elsevier, pp 1403–1415. <https://doi.org/10.1016/j.istruc.2022.08.055>
- Ping Q, Fang Z, Ma D, Zhang H (2020) Coupled static-dynamic tensile mechanical properties and energy dissipation characteristic of limestone specimen in SHPB tests. In: *Advances in civil engineering, 2020*
- Yang F, Ma H, Jing L, Zhao L, Wang Z (2015) Dynamic compressive and splitting tensile tests on mortar using split Hopkinson pressure bar technique. *Latin Am J Solids Struct* 12:730–746. <https://doi.org/10.1590/1679-78251513>
- Chen X, Wu S, Zhou J (2014) Quantification of dynamic tensile behavior of cement-based materials. *Constr Build Mater* 51:15–23. <https://doi.org/10.1016/j.conbuildmat.2013.10.039>
- Ahmad S, Bhargava P, Chourasia A, Usmani A (2020) Effect of elevated temperatures on the shear-friction behaviour of concrete: experimental and analytical study. *Eng Struct* 225:111305. <https://doi.org/10.1016/j.engstruct.2020.111305>
- Ahmad S, Bhargava P, Bhandari NM (2018) Evaluation of shear transfer capacity of reinforced concrete exposed to fire. In: 12th fib International Ph.d. symposium in civil engineering. Czech Technical University
- Ahmad S, Bhargava P, Chourasia A (2020) Direct shear failure in concrete joints exposed to elevated temperatures. In: *Structures*, vol 27. Elsevier, pp 1851–1859. <https://doi.org/10.1016/j.istruc.2020.07.074>
- Ahmad S, Bhargava P, Chourasia A, Ju M (2021) Residual shear strength of reinforced concrete slender beams without

- transverse reinforcement after elevated temperatures. *Eng Struct* 237:112163. <https://doi.org/10.1016/j.engstruct.2021.112163>
36. IS: 10262:2019 Concrete Mix Proportioning—Guidelines
  37. IS: 456:2000 Plain and Reinforced Concrete Code of Practice
  38. IS 516: 1959 Methods of Tests for Strength of Concrete
  39. Kolsky H (1949) An investigation of the mechanical properties of materials at very high rates of loading. *Proc Phys Soc* 162(11):676. <https://doi.org/10.1088/0370-1301/62/11/302>
  40. Khan MM, Iqbal MA (2023) Design, development, and calibration of split Hopkinson pressure bar system for Dynamic material characterization of concrete. *Int J Protect Struct*. <https://doi.org/10.1177/20414196231155947>
  41. Khan MM, Iqbal MA (2023) Dynamic response of concrete subjected to high rate of loading: a parametric study. *Mech Solids* 58:1378–1394. <https://doi.org/10.3103/S0025654423600915>
  42. Cao S, Yilmaz E, Song W (2018) Dynamic response of cement-tailings matrix composites under SHPB compression load. *Constr Build Mater* 186:892–903. <https://doi.org/10.1016/j.conbuildmat.2018.08.009>
  43. Khan MM, Iqbal MA (2023) Strain rate and size effects on dynamic compressive behaviour of standard and high-strength concrete. *Mater Struct* 56:176. <https://doi.org/10.1617/s11527-023-02266-x>
  44. (1990) *Comite Euro-International du Beton-Federation Internationale de la Precontrainte*. CEB-FIP Model Code 90 Redwood Books, Trowbridge, Wiltshire, Great Britain
  45. Tedesco JW, Ross CA (1998) Strain-rate-dependent constitutive equations for concrete. *J Pressure Vessel Technol* 398:405. <https://doi.org/10.1115/1.2842350>
  46. Zhou XQ, Hao H (2008) Modelling of compressive behaviour of concrete-like materials at high strain rate. *Int J Solids Struct* 45(17):4648–4661. <https://doi.org/10.1016/j.ijsolstr.2008.04.002>
  47. Grote DL, Park SW, Zhou M (2001) Dynamic behavior of concrete at high strain rates and pressures: I. Experimental characterization. *Int J Impact Eng* 25(9):869–886. [https://doi.org/10.1016/S0734-743X\(01\)00020-3](https://doi.org/10.1016/S0734-743X(01)00020-3)
  48. Katayama M, Itoh M, Tamura S, Beppu M, Ohno T (2007) Numerical analysis method for the RC and geological structures subjected to extreme loading by energetic materials. *Int J Impact Eng* 34(9):1546–1561. <https://doi.org/10.1016/j.ijimpeng.2006.10.013>
  49. Li QM, Lu YB, Meng H (2009) Further investigation on the dynamic compressive strength enhancement of concrete-like materials based on split Hopkinson pressure bar tests Part II: numerical simulations. *Int J Impact Eng* 36(12):1335–1345. <https://doi.org/10.1016/j.ijimpeng.2009.04.010>
  50. Chen J, Zhuang J, Shen S, Dong S (2022) Experimental investigation on the impact resistance of rubber self-compacting concrete. In: *Structures*, vol 39. Elsevier, pp 691–704. <https://doi.org/10.1016/j.istruc.2022.03.057>
  51. Xie H, Yang L, Zhu H, Zhang Q, Deng X, Wei P, Lü J (2022) Energy dissipation and fractal characteristics of basalt fiber reinforced concrete under impact loading. In: *Structures*, vol 46. Elsevier, pp 654–663. <https://doi.org/10.1016/j.istruc.2022.10.086>
  52. Wu M, Qin C, Zhang C (2014) High strain rate splitting tensile tests of concrete and numerical simulation by mesoscale particle elements. *J Mater Civ Eng* 26(1):71–82. [https://doi.org/10.1061/\(ASCE\)MT.1943-5533.0000776](https://doi.org/10.1061/(ASCE)MT.1943-5533.0000776)
  53. Soroushian P, Choi KB, Alhamad A (1986) Dynamic constitutive behavior of concrete. *J Proc* 83(2):251–259. <https://doi.org/10.14359/10423>
  54. Komlos K (1970) Investigation of rheological properties of concrete in uniaxial tension. *Mater Test* 12(9):300–304
  55. Xiao S, Li H, Monteiro PJM (2010) Influence of strain rates and load histories on the tensile damage behaviour of concrete. *Mag Concr Res* 62(12):887–894. <https://doi.org/10.1680/macr.2010.62.12.887>

Springer Nature or its licensor (e.g. a society or other partner) holds exclusive rights to this article under a publishing agreement with the author(s) or other rightsholder(s); author self-archiving of the accepted manuscript version of this article is solely governed by the terms of such publishing agreement and applicable law.